

Solving the Einstein Equations Numerically

David Hilditch

Abstract There are many complementary approaches to the construction of solutions to the field equations of general relativity. Among these, numerical approximation offers the only possibility to compute a variety of dynamical spacetimes, and so has come to play an important role for theory and experiment alike. Presently we give a brief introduction to this, the science of numerical relativity. We discuss the freedom in formulating general relativity as an initial (boundary) value problem. We touch on the fundamental concepts of well-posedness and gauge freedom and review the standard computational methods employed in the field. We discuss the physical interpretation of numerical spacetime data and end with an overview of a number of 3d codes that are either in use or under active development.

1 Overview

This book is primarily concerned with advanced computational methods for general relativistic magnetohydrodynamics (GRMHD) and the solutions they produce. It is therefore assumed at the outset that the reader already has a solid grasp of the fundamentals of general relativity (GR) [1]. There are, however, many practitioners working on GRMHD who enter the subject through computational astrophysics, where it is common to solve the field equations of GRMHD with a given, fixed, spacetime metric. Following on from the previous Chapter [2], in which a concise overview to GRMHD was given, our purpose here is to give a brief introduction to the field of numerical relativity (NR), where the metric becomes an additional dependent variable. There are excellent textbooks [3, 4, 5, 6, 7], which are highly recommended for those seeking instead a complete introduction to the topic.

David Hilditch (✉)

CENTRA, Departamento de Física, Instituto Superior Técnico – IST, Universidade de Lisboa – UL, Avenida Rovisco Pais 1, 1049-001 Lisboa, Portugal, e-mail: david.hilditch@tecnico.ulisboa.pt

Starting with the basics, we recall that in GR, gravitation is described geometrically within the spacetime manifold M as the curvature of the Levi-Civita covariant derivative ∇_a associated with the Lorentzian metric g_{ab} , which we take to have mostly plus signature. The goal of the relativist is then to understand the solution space of Einstein's equations, the field equations of the theory,

$${}^{(4)}G_{ab} \equiv {}^{(4)}R_{ab} - \frac{1}{2}g_{ab}{}^{(4)}R = 8\pi T_{ab}, \quad (1)$$

expressed here and throughout in units with $G = c = 1$. Latin indices starting from the beginning of the alphabet will be abstract, and we shall work in the physical $3+1$ dimensions. The label (4) denotes then the spacetime curvature, distinct from the spatial curvature introduced below. The generalization of the results presented in this Chapter to higher or lower spacetime dimensions is straightforward. The Ricci tensor and scalar are given, respectively by,

$${}^{(4)}R_{ab} = {}^{(4)}R_{acb}{}^c, \quad {}^{(4)}R = g^{ab}{}^{(4)}R_{ab}, \quad (2)$$

with the inverse metric denoted as usual by g^{ab} . Introducing coordinates x^μ and writing out the field equations in the associated coordinate basis we obtain a system of coupled nonlinear partial differential equations (PDEs) whose solution space we can first try to understand with various simplifying strategies. Under strong symmetry assumptions, for instance, we may be able to find exact analytic solutions. The most important of these for the astrophysics of black holes is the Kerr solution. If we are interested in physical scenarios that are close to a known solution, we may linearize about that background and solve these simplified equations, whose solutions nevertheless accurately describe the physics of interest. This approach is fundamental to understand the propagation of weak gravitational waves far from their original source. More generally, when we encounter a problem with two or more very different scales we can use the smaller of the two as an expansion parameter. This strategy is used in the self-force treatment of extreme mass-ratio compact binary systems and in the Post-Newtonian expansion of the field equations, which has proven highly successful in the computation of the inspiral motion of compact binary systems. Turning instead to produce and understand solutions to the full field equations without simplifying assumptions, methods of pure mathematical analysis are absolutely fundamental to obtain a rigorous picture. Yet the general message we must absorb from the PDE literature is that such pure analysis will not provide solutions *in hand*. In many physical applications however, we do need the solution itself. To overcome this we turn to NR: the use of numerical methods to find approximate solutions to the field equations that converge to solutions of the continuum equations in the limit of infinite resolution. We will see that the requirement of convergence guides much of the theory in the topic. The most important application of NR to astrophysics is in the computation of the late stages of compact binary inspiral and merger.

In the following we give an overview of the basics of NR. We begin in Section 2 by reviewing the formulation of GR as an initial value and initial boundary value problem. We discuss well-posedness and the most popular free-evolution formula-

tions of GR. In Section 3 the post-processing used to give physical interpretation to numerically constructed spacetime data is discussed. Finally, in Section 4 we give an introduction to the standard methods used in NR, and finally give an overview of the 3d codes in use.

2 Formulations of GR

Perhaps the single most important insight of special and general relativity is that space and time should be viewed as a unified entity. Using this insight to express field theories of interest results in a minimal and elegant formulation of their field equations. Yet such a spacetime formulation is not optimally adapted to the treatment of the initial and initial boundary value problems that necessarily underpin any understanding of dynamics within the theory. Textbook numerical methods for time evolution moreover rely on a clear separation of temporal and spatial derivatives. In this section, focusing primarily on the evolution of the metric in GR, we review the 3 + 1 decomposition, which allows this separation. Afterwards we move on to discuss free-evolution, well-posedness and gauge freedom as they are usually framed in the NR literature.

2.1 The 3+1 Split

Suppose that we are given a solution to Einstein's equations (1) expressed in coordinates x^μ in a coordinate patch. Then we may map from an abstract tensor $T_{a_1 \dots a_k}{}^{b_1 \dots b_l}$ to the components $T_{\mu_1 \dots \mu_k}{}^{\nu_1 \dots \nu_l}$ in the coordinate basis defined by ∂_α^a and $\nabla_a x^\mu$ simply by contracting on every abstract index with elements of the basis,

$$T_{\mu_1 \dots \mu_k}{}^{\nu_1 \dots \nu_l} = T_{a_1 \dots a_k}{}^{b_1 \dots b_l} (\partial_{\mu_1}^{a_1} \dots \partial_{\mu_k}^{a_k}) (\nabla_{b_1} x^{\nu_1} \dots \nabla_{b_l} x^{\nu_l}). \quad (3)$$

Likewise the tensor itself can be reconstructed from the components using

$$T_{a_1 \dots a_k}{}^{b_1 \dots b_l} = T_{\mu_1 \dots \mu_k}{}^{\nu_1 \dots \nu_l} (\nabla_{a_1} x^{\mu_1} \dots \nabla_{a_l} x^{\mu_l}) (\partial_{\nu_1}^{b_1} \dots \partial_{\nu_l}^{b_l}). \quad (4)$$

We suppose now that $x^\mu = (t, x^i)$ with level sets Σ_t of t spacelike, in the sense that vectors tangent to Σ_t are spacelike. We then refer to t as a time coordinate. The collection of level sets Σ_t is called a foliation of the spacetime. Individual level sets are equivalently referred to as either instants of time or slices. We define the lapse function α by,

$$\alpha^{-2} = -g^{ab} \nabla_a t \nabla_b t. \quad (5)$$

We may now define the future directed unit normal to slices of constant t by

$$n^a = -\alpha \nabla^a t. \quad (6)$$

We define a projection operator through

$$\perp^a{}_b = \delta^a{}_b + n^a n_b. \quad (7)$$

The lapse measures the proper time elapsed between neighboring slices of the foliation. Direct computation reveals that $\perp^a{}_c \perp^c{}_b = \perp^a{}_b$, so that this indeed defines a projection. The core idea of the 3 + 1 decomposition is that we should never deal directly with general tensors. Instead, we decompose all tensors into a set of objects that exist naturally within the foliation. For example, given a general vector field v^a , we may define,

$$v^n \equiv v^a n_a, \quad (\perp v)^a \equiv \perp^a{}_b v^b. \quad (8)$$

The vector field can be reconstructed from its normal v^n and spatial $(\perp v)^a$ components

$$v^a = (\perp v)^a - n^a v^n. \quad (9)$$

The spatial part of the vector is orthogonal to the normal vector $(\perp v)^a n_a = 0$. The generalization of this decomposition to higher rank tensors follows the obvious pattern. Any tensor which is orthogonal to n^a on every index is called spatial. Since the normal vector depends upon the time coordinate, this definition is made with respect to a foliation. Consequently every spatial vector is spacelike, but not vice-versa. Our task now is to apply the idea of decomposition to the objects that appear in GR.

These objects may be naturally organized in a hierarchy according to the number of derivatives that they (implicitly) contain. At zeroth order we have the coordinates $x^\mu = (t, x^i)$. Then at first order we have the metric g_{ab} , the coordinate basis vectors $\partial_\alpha^a = (\partial_t^a \equiv t^a, \partial_i^a \equiv \partial_{x^i}^a)$ and the basis one-forms dx^μ (which can also be written $\nabla_a x^\mu$). Recall that, by definition, we have the relationships

$$\delta^a{}_b = \partial_\alpha^a \nabla_b x^\alpha, \quad \delta^\alpha{}_\beta = \partial_\beta^a \nabla_a x^\alpha = \partial_\beta x^\alpha, \quad (10)$$

which we use without further comment in the manipulations below. Next are the connection coefficients ${}^{(4)}\Gamma^\alpha{}_{\mu\nu}$, and at third order, or equivalently with two derivatives of the metric, the curvature ${}^{(4)}R_{abcd}$. Finally for our present needs, the second Bianchi identities

$$\nabla_{[a} {}^{(4)}R_{bc]de} = 0, \quad (11)$$

and any contractions thereof lie at the fourth level. We treat each level of this hierarchy in turn.

There is nothing to do to treat the coordinates $x^\mu = (t, x^i)$ as they constitute a collection of scalar fields rather than a tensor.

Moving on the first level, the basis vectors decompose as,

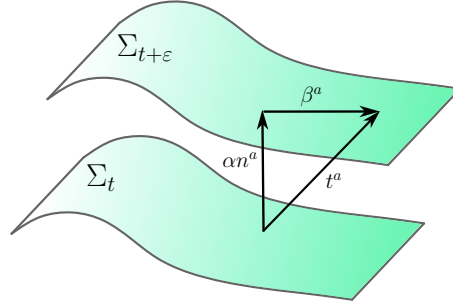


Fig. 1: Level sets Σ_t and neighbor $\Sigma_{t+\epsilon}$ of the foliation, together with a depiction of the relationship between the time vector t^a , the lapse function α , the shift vector β^a , and the future pointing unit normal to slices of the foliation n^a .

$$\begin{aligned} t^a n_a &= -\alpha, & \perp t^a &\equiv \beta^a, \\ \partial_i^a n_a &= 0, & \perp \partial_i^a &= \partial_i^a, \end{aligned} \quad (12)$$

where here and in what follows we adopt the convention that the appearance of the projection operator without indices means projection on all open abstract indices on the object directly to the right of it. We have defined the shift vector β^a as the spatial part of the time vector t^a . It encodes the difference between the integral curves of the time vector and the normal vector. Rearranging, we have

$$t^a = \alpha n^a + \beta^a, \quad \partial_i^a = \perp \partial_i^a \quad (13)$$

and, unsurprisingly, we see that the ‘spatial derivatives’ ∂_i are spatial according to our definition without projection. The basis one-forms dx^i are then given by,

$$\begin{aligned} n^a \nabla_a t &= \alpha^{-1}, & \perp \nabla_a t &= 0, \\ n^a \nabla_a x^i &= -\alpha^{-1} \beta^i, & \perp \nabla_a x^i &= \gamma_a^b \nabla_a x^i = \gamma_a^i. \end{aligned} \quad (14)$$

These relationships may be rewritten as,

$$\nabla_a t = -\alpha^{-1} n_a, \quad \nabla_a x^i = \alpha^{-1} \beta^i n_a + \perp \nabla_a x^i. \quad (15)$$

The geometry of the foliation and the relationship between the normal and time vectors is sketched in Fig. 1. The metric decomposes as

$$g_{mn} = -1, \quad \perp g_{an} = 0, \quad \gamma_{ab} = \perp g_{ab} = \perp_{ab} = g_{ab} + n_a n_b. \quad (16)$$

In the last expressions here we define the spatial metric, which may be thought of geometrically as a metric on slices of the foliation induced by g_{ab} . Clearly the spatial metric is positive definite when acting on spatial vectors $\gamma_{ab} v^a v^b \geq 0$. Observe that

within the $3 + 1$ split, the metric is special because it was used to define the unit normal vector n^a . Consequently rearranging (16), we arrive at a particularly simple expression

$$g_{ab} = \gamma_{ab} - n_a n_b. \quad (17)$$

Nevertheless, observe that the decomposition of the metric itself used the approach sketched above in a completely boiler-plate manner.

If we work in the coordinate basis ∂_α^a , spatial tensors take a particularly simple form. Consider once more an arbitrary spatial vector v^a . Expanding out the orthogonality condition $v^a n_a = 0$, we find,

$$0 = v^a n_a = -v^0 \alpha, \quad (18)$$

which means that the time component of a spatial vector must vanish $v^0 = 0$ at any point where the foliation has non-vanishing lapse. For an arbitrary spatial covector, we instead have

$$0 = n^a v_a = \alpha^{-1} v_0 - \alpha^{-1} \beta^i v_i, \quad (19)$$

which means that the time component is given by the inner product with the shift vector, which is itself spatial, so that so long as the lapse is bounded we have,

$$v_0 = \beta^i v_i. \quad (20)$$

The generalization of this result to tensors of arbitrary valence is straightforward. We conclude that, in a regular foliation with finite non-vanishing lapse, if we know the shift vector, then the spatial components of an arbitrary spatial tensor suffice to reconstruct the full tensor. We will use this to express the full Einstein equations in our coordinate basis below after the remainder of the geometric decomposition.

In the second level of the hierarchy we need to obtain a complete representation of the connection ∇_a . For the reasons discussed in the last paragraph, we need only know how to compute derivatives of spatial tensors within the $3 + 1$ formalism. Given an arbitrary spatial tensor we define the spatial covariant derivative by total projection of the spacetime covariant derivative

$$D_a T_{a_1 \dots a_k}{}^{b_1 \dots b_l} = \perp \nabla_a T_{a_1 \dots a_k}{}^{b_1 \dots b_l}. \quad (21)$$

It turns out that the spatial covariant derivative is nothing more than the Levi-Civita derivative of the spatial metric. This can be verified by verifying first that it is torsion free

$$2D_{[a} D_{b]} \phi = 2 \perp \nabla_{[a} (\nabla_{b]} \phi + n_{b]} \mathcal{L}_n \phi) = 2 \perp \nabla_{[a} n_{b]} \mathcal{L}_n \phi = 0. \quad (22)$$

Here the last term vanishes by Frobenius theorem because n^a is hypersurface orthogonal, square parentheses $[]$ on indices denote antisymmetrization with the usual normalization of [1], and we employ the standard notation for the Lie-derivative.

Second, we see that it is compatible with the spatial metric,

$$D_a \gamma_{bc} \equiv \perp \nabla_a (g_{bc} + n_b n_c) = 0. \quad (23)$$

Observe that with this definition the spatial coordinate basis from (15) can be rewritten as $\nabla_a x^i = \alpha^{-1} \beta^i n_a + D_a x^i$. To capture pieces of the projected covariant derivative $\perp^c \nabla_c T_{a_1 \dots a_k}{}^{b_1 \dots b_l}$ normal to the level set Σ_t we need a representation of derivatives of n_a . For this we define the acceleration vector a_a and the extrinsic curvature K_{ab} , which are given, respectively, by

$$a_a = n^b \nabla_b n_a, \quad K_{ab} = -\gamma^c{}_a \nabla_c n_b. \quad (24)$$

Both are spatial by virtue of the unit normalization of n^a . One should be aware that in the mathematics literature the extrinsic curvature is occasionally defined with the opposite sign convention. As in Eq. (22), hypersurface orthogonality of n_a simplifies matters, allowing us to rewrite $a_a = D_a \ln \alpha$. The covariant derivative of n_a is completely represented through these variables and can now be expressed as

$$\nabla_a n_b = -K_{ab} - n_a a_b. \quad (25)$$

The same argument given below equation (22) shows that the extrinsic curvature is symmetric. Using orthogonality of n^a with spatial $T_{a_1 \dots a_k}{}^{b_1 \dots b_l}$ it follows that

$$n^{a_1} \perp^c \nabla_c T_{a_1 \dots a_k}{}^{b_1 \dots b_l} = -(\perp^c \nabla_c n^{a_1}) T_{a_1 \dots a_k}{}^{b_1 \dots b_l} = K_a{}^{a_1} T_{a_1 \dots a_k}{}^{b_1 \dots b_l}, \quad (26)$$

and likewise with the contraction with n^a on any slot within the derivative, so that we now have a complete representation of any covariant derivative of a spatial tensor projected with \perp on the derivative index itself. The extrinsic curvature plays yet another role, however, as it can be viewed morally as a ‘time derivative’ of the spatial metric, through the relation

$$K_{ab} = -\frac{1}{2} \mathcal{L}_n \gamma_{ab}. \quad (27)$$

There is variability in the literature in the representation of the ‘time derivative’ of an arbitrary spatial tensor under the 3 + 1 split that depends on the specific equations under consideration, but this serves as the canonical example. The core idea is always to introduce the Lie derivative along a vector field with non-vanishing contraction with n^a as a dependent variable, and then project the resulting object on every remaining open index. For instance for $T_{a_1 \dots a_k}{}^{b_1 \dots b_l}$, we might introduce

$$S_{a_1 \dots a_k}{}^{b_1 \dots b_l} = \perp \mathcal{L}_n T_{a_1 \dots a_k}{}^{b_1 \dots b_l}. \quad (28)$$

The remainder of the Lie-derivative of $T_{a_1 \dots a_k}{}^{b_1 \dots b_l}$ along n^a is given by relationships akin to equation (26) but with the acceleration a_a playing the role of the extrinsic curvature. Again contracting on the first index of a given type as a representative example, we have,

$$n^{a_1} \mathcal{L}_n T_{a_1 \dots a_k}{}^{b_1 \dots b_l} = 0, \quad (29)$$

when the contraction is made with any index downstairs, and

$$n_{b_1} \mathcal{L}_n T_{a_1 \dots a_k}{}^{b_1 \dots b_l} = -a_{b_1} T_{a_1 \dots a_k}{}^{b_1 \dots b_l}. \quad (30)$$

otherwise. In fact we have now introduced enough variables to achieve a complete description of the connection coefficients in our coordinate basis. To verify this we simply use the general definition,

$${}^{(4)}\Gamma^\alpha{}_{\mu\nu} = \partial_\mu^a (\nabla_a \partial_\nu^b) \nabla_b x^\alpha, \quad (31)$$

express our basis vectors as in (13), and (15), and collect all possible contractions and projections, which results in

$$\begin{aligned} {}^{(4)}\Gamma^n{}_{nm} &= -\partial_n \ln \alpha, \\ {}^{(4)}\Gamma^n{}_{in} &= -a_i = -\partial_i \ln \alpha, \\ {}^{(4)}\Gamma^\alpha{}_{nm} \perp^i{}_\alpha &= \alpha^{-1} \partial_n \beta^i + a^i, \\ {}^{(4)}\Gamma^\alpha{}_{in} \perp^j{}_\alpha &= \alpha^{-1} \partial_i \beta^j - K_i{}^j, \\ {}^{(4)}\Gamma^n{}_{ij} &= K_{ij}, \\ {}^{(4)}\Gamma^\alpha{}_{ij} \perp^k{}_\alpha &= \partial_i^a (D_a \partial_j^b) D_b x^k \equiv \Gamma^k{}_{ij}. \end{aligned} \quad (32)$$

Observe that, despite the name, the extrinsic curvature really belongs to the connection. We realized already above that the spatial covariant derivative is the Levi-Civita covariant derivative of the spatial metric. It follows that the spatial connection coefficients $\Gamma^k{}_{ij}$ are just the associated Christoffel symbols,

$$\Gamma^k{}_{ij} = \frac{1}{2} \gamma^{kl} (\partial_i \gamma_{jl} + \partial_j \gamma_{il} - \partial_l \gamma_{ij}). \quad (33)$$

In a coordinate basis the spacetime connection coefficients ${}^{(4)}\Gamma^\alpha{}_{\mu\nu}$ have 40 algebraically independent components. Taking into account the symmetry of K_{ij} and $\Gamma^k{}_{ij}$ in the downstairs indices and adding the number of components of each line of (32), we have $1 + 3 + 3 + 9 + 6 + 18 = 40$, confirming that we have captured the spacetime object completely.

We now move on to the third level in our derivative hierarchy, the geometric decomposition of curvature quantities. In 3 + 1 dimensions there are 20 algebraically independent components of the spacetime Riemann curvature ${}^{(4)}R_{abcd}$, and we therefore seek 20 algebraically independent equations upon decomposition. In other words; symmetries of the Riemann tensor vastly reduce the number of different contractions and projections we must consider. We start by projecting on every index, which reveals,

$$\perp {}^{(4)}R_{abcd} = R_{abcd} + 2K_{a[c} K_{d]b}. \quad (34)$$

Here we have introduced the spatial Riemann tensor R_{abcd} , the curvature associated with the spatial covariant derivative, defined as usual through commutation,

$$2D_{[a}D_{b]}w_c = R_{abc}{}^d w_d, \quad (35)$$

with w_a an arbitrary spatial one-form. Equation (34) is known as the Gauss equation. It is straightforwardly derived by contracting ${}^{(4)}R_{abcd}$ on the last index with an arbitrary spatial vector, projecting on the remaining indices and using the definition of the spatial covariant derivative D_a and extrinsic curvature K_{ab} . Recall that, although we are using abstract spacetime indices, since we work with spatial tensors we need only count their spatial components. In 3 dimensions the Riemann tensor has 6 algebraically independent components. A useful expression of this fact is that in the $3+1$ setting the spatial Riemann tensor R_{abcd} is determined entirely by the spatial Ricci tensor $R_{ab} = R_{acb}{}^c$ and its trace, the spatial Ricci scalar $R = \gamma^{ab}R_{ab}$,

$$R_{abcd} = 2(\gamma_{[c}R_{d]b} - \gamma_{b[c}R_{d]a}) - R\gamma_{a[c}\gamma_{d]b}, \quad (36)$$

which can also be viewed as the fact that in 3 dimensions the Weyl tensor vanishes identically. Next we have the Codazzi-Mainardi equations, which are built by contracting once with the normal vector n^a before projecting on the remaining indices, giving

$$\perp {}^{(4)}R_{abcd}n^d = -2D_{[a}K_{b]c}. \quad (37)$$

The derivation of this result follows the exact same pattern sketched above for the Gauss equation. Counting here is a little more subtle. For each of the 3 independent components of the index without symmetrization, there are 3 equations associated with the antisymmetrized indices, giving a total of 9 equations. But the totally antisymmetric part also vanishes by the first spacetime Bianchi identity ${}^{(4)}R_{[abc]d} = 0$. In 3 dimensions this amounts to one more equation that we must subtract, giving 8 algebraically independent components in total in (37). The same combination of contractions and projections can in fact be used together with the Bianchi identity to efficiently obtain an evolution equation for the spatial connection coefficients, but this not needed presently. Finally, the Ricci equations are obtained by contracting twice with the normal vector and projecting on the remaining indices, which gives

$$\perp {}^{(4)}R_{abcd}n^b n^d = \mathcal{L}_n K_{ab} + \alpha^{-1} D_a D_b \alpha + K^c{}_a K_{bc}, \quad (38)$$

again by following the procedure sketched above. The symmetries of the Riemann tensor actually make the projection superfluous, but maintaining it makes counting more transparent. Since we have now a symmetric spatial tensor, there are 6 algebraically independent components here. Double-checking, from (34), (37) and (38) we have a total of $6 + 8 + 6 = 20$ algebraically independent components, as required.

Moving now to the fourth level of the hierarchy, the highest that we require here, the decomposition of the second Bianchi identities (11) proves useful. These correspond to algebraically 20 independent equations, with four independent contractions

of interest. We begin by projecting on every index, which reveals the second Bianchi identity for D_a ,

$$0 = \perp \nabla_{[a} {}^{(4)}R_{bc]de} = D_{[a} R_{bc]de}, \quad (39)$$

which could also be viewed as a consequence of the fact that the spatial covariant derivative is itself torsion-free, again as a result of the fact that n^a is hypersurface orthogonal. These correspond to 3 equations, consistent with the number of contracted Bianchi identities in 3 dimensions, which can be seen by substitution of (36) into (39). Next we contract with the normal vector on one of the non-explicitly antisymmetrized indices and project the rest. This gives

$$0 = -\perp \nabla_{[a} {}^{(4)}R_{bc]de} n^e = 2D_{[a} D_b K_{c]d} - K^e{}_{[a} R_{bc]de}, \quad (40)$$

which contains another 3 algebraically independent equations. Viewed from the perspective of the spatial covariant derivative, this identity holds simply by the definition of the spatial Riemann curvature and the Bianchi identity (39). Contracting instead with the normal vector on the antisymmetrized indices and projecting, we have

$$\begin{aligned} 0 &= 3 \perp \nabla_{[a} {}^{(4)}R_{bc]de} n^a \\ &= \perp \mathcal{L}_n (\perp {}^{(4)}R_{bcde}) - 2 \perp {}^{(4)}R_{bca[d} K_{e]}^a + 2\gamma^{fg} \perp {}^{(4)}R_{feg[b} K_{c]d} - 2\gamma^{fg} \perp {}^{(4)}R_{fdg[b} K_{c]e} \\ &\quad - 2D_b (D_{[d} K_{e]c}) + 2D_c (D_{[d} K_{e]b}) + 4(D_{[d} K_{e][b} a_{c]} + 4(D_{[b} K_{c][d} a_{e]}) \\ &\quad + 2 \perp {}^{(4)}R_{d[b} K_{c]e} - 2 \perp {}^{(4)}R_{e[b} K_{c]d}, \end{aligned} \quad (41)$$

which encodes 6 equations. In this equation, for brevity, we have not expanded out $\perp {}^{(4)}R_{abcd}$ from (34). Finally, we contract once with the unit normal in each of the two blocks of indices,

$$\begin{aligned} 0 &= 3 \perp \nabla_{[a} {}^{(4)}R_{bc]de} n^a n^e \\ &= -2 \perp \mathcal{L}_n (D_{[b} K_{c]}^e) \gamma_{de} + 2K D_{[b} K_{c]d} + K_c^e (2D_{[d} K_{e]b} - D_b K_{de} + D_b (\gamma_{de} K)) \\ &\quad - 2K_b^e D_{[d} K_{e]c} + 2D_{[b} R_{c]d} + K_{eb} D_c K_{de} - K_{bd} D_c K + 2a_{[b} (R_{c]d} + K_{c]d} K - K_{c]}^e K_{de}) \\ &\quad - a^e (R_{bcde} + 2K_{b[d} K_{e]c}) - 2^{-1} D_{[b} (\perp {}^{(4)}R_{c]d}) - 2a_{[b} \perp {}^{(4)}R_{c]d}, \end{aligned} \quad (42)$$

which results in the remaining 8 algebraically independent equations.

To this point our discussion was entirely geometrical. Given a spacetime manifold M , Lorentzian metric g_{ab} with an associated Levi-Civita connection ∇_a , coordinates $x^\mu = (t, x^i)$ whose time coordinate t has spacelike level sets and associated coordinate basis vectors ∂_α , and one-forms dx^μ , we have understood how to rewrite the geometry in a 3 + 1 decomposed form. We now use this formalism to reformulate Einstein's equations (1). For this we could apply our recipe above in a purely agnostic fashion to the field equations. But to streamline the derivation it is convenient to begin with the observation that in 3 + 1 dimensions the Einstein tensor can be decomposed in the form

$$G_{ab} = G_{nn}(n_a n_b + \gamma_{ab}) + 2n_{(a} \perp G_{b)n} + \perp^{(4)} R_{ab} - \gamma_{ab} {}^{(4)} R_{cd} \gamma^{cd}, \quad (43)$$

where round parentheses () on indices denote symmetrization with the usual normalization of [1]. Thus we may consider the three pieces G_{nn} , $\perp G_{an}$ and $\perp^{(4)} R_{ab}$. We define variables for the decomposition of the stress-energy tensor, namely

$$\rho = T_{ab} n^a n^b, \quad j_a = -\perp T_{ab} n^b, \quad s_{ab} = \perp T_{ab}. \quad (44)$$

the energy density, momentum density and spatial stress tensors, respectively, as viewed by normal observers who travels along integral curves of n^a . Straightforward application of the 3 + 1 decomposition on G_{nn} then reveals the first of the field equations as

$$H = 2G_{nn} - 16\pi T_{nn} = R + K^2 - K^{ab} K_{ab} - 16\pi \rho = 0. \quad (45)$$

Observe that no explicit time derivatives occur here (in this formalism these would occur in the form \mathcal{L}_n). For this reason, this equation constraints the permissible data at any instant of time Σ_t . It is called the Hamiltonian constraint. Taking now the $\perp G_{an}$ and using a trace of the Codazzi-Mainardi formula (37) we obtain,

$$M_a = -\perp G_{an} = D^b K_{ab} - D_a K - 8\pi j_a = 0. \quad (46)$$

Again, there are no explicit time derivatives and so these equations restrict permissible data at all times. This is known as the momentum constraint. For the last piece $\perp^{(4)} R_{ab}$, we project the trace-reversed Einstein equations, obtaining

$$\begin{aligned} \mathcal{L}_n K_{ab} = & -\alpha^{-1} D_a D_b \alpha + R_{ab} - 2K^c{}_a K_{bc} + K K_{ab} \\ & + 8\pi \left[s_{ab} - \frac{1}{2} \gamma_{ab} s + \frac{1}{2} \gamma_{ab} \rho \right], \end{aligned} \quad (47)$$

These are now true evolution equations which, in some sense, encode the dynamical behavior of GR.

It remains to offer a little tidying up. Observe that the Einstein equations do not determine the time evolution of γ_{ab} but rather that of the extrinsic curvature. This is no problem, however, since (27) already told us that the extrinsic curvature can be viewed as the time derivative of the metric. For practical numerical purposes we need to express the field equations not as Lie derivatives of abstract index tensors but directly with partial derivatives of their components. This is easily achieved by using the relation (13) to replace the normal vector with the time vector t^a and expanding out the equations in our coordinate basis. Doing so, we finally arrive at the Arnowitt-Deser-Misner (ADM), or York, evolution equations,

$$\begin{aligned} \partial_t \gamma_{ij} = & -2\alpha K_{ij} + \mathcal{L}_\beta \gamma_{ij}, \\ \partial_t K_{ij} = & -D_i D_j \alpha + \alpha \left[R_{ij} - 2K^k{}_i K_{jk} + K K_{ij} \right] \\ & + 4\pi \alpha \left[\gamma_{ij} (s - \rho) - 2s_{ij} \right] + \mathcal{L}_\beta K_{ij}. \end{aligned} \quad (48)$$

We make the usual abuse of notation when expressing derivatives, in a basis, writing

$$D_i D_j \alpha \equiv (\partial_i^a \partial_j^b) D_a D_b \alpha, \quad \mathcal{L}_\beta \gamma_{ij} \equiv (\partial_i^a \partial_j^b) \mathcal{L}_\beta \gamma_{ab}, \quad (49)$$

and so forth. If we take a divergence of the Einstein equations, the left-hand side vanishes identically, giving $\nabla^b T_{ab} = 0$, which can be interpreted as the local conservation of energy and momentum. Under the 3 + 1 decomposition these four equations can be written as

$$\begin{aligned} \partial_t \rho &= \alpha [D^i j_i + 2a^i j_i - K\rho - K^{ij} s_{ij}] + \mathcal{L}_\beta \rho, \\ \partial_t j_i &= -\alpha [D^j s_{ij} + a^j s_{ij} - K j_i + a_i \rho] + \mathcal{L}_\beta j_i. \end{aligned} \quad (50)$$

Observe that the lapse and shift are completely absent from the constraints, and furthermore that they have no equations of motion. Instead, they encode the freedom in the choice of coordinates. In NR this is usually viewed as the gauge freedom of the theory. We asserted above that the Hamiltonian (45) and momentum (46) constraints restrict the permissible data at each instant of time. This can only be self-consistent if the evolution equations (48) respect the constraints, in the sense that the time development of constraint-satisfying initial data remains constraint-satisfying. It turns out that, under the evolution equations (48), the constraints evolve according to the formal evolution system

$$\begin{aligned} \partial_t H &= -2\alpha D^i M_i - 4M^i D_i \alpha + 2\alpha KH + \mathcal{L}_\beta H, \\ \partial_t M_i &= -\frac{1}{2}\alpha D_i H + \alpha K M_i - (D_i \alpha) H + \mathcal{L}_\beta M_i. \end{aligned} \quad (51)$$

These equations can be obtained, for instance, by taking suitable traces of (41) and (42), plugging in the Einstein equations and using (50), or equivalently by 3 + 1 decomposition of the spacetime contracted Bianchi identities. Obviously $H = M_a = 0$ is a solution to these equations. Therefore given constraint satisfying initial data that can be evolved in time, there ought to be at least one solution that is constraint satisfying.

Putting aside for now any subtleties associated with the stress-energy tensor, we can now give a complete geometric formulation of the initial value (Cauchy) problem for GR. At an instant of time Σ_t we choose (γ_{ab}, K_{ab}) satisfying the Hamiltonian and momentum constraints, which then evolve according to the evolution system (48). This leads to the concept of free-evolution in NR, in which the idea is to solve the constraints just once for initial data and then evolve those data in time, relying on closure of the constraint subsystem to guarantee they are satisfied at later times. In practice numerical error violates the constraints, but these violations should converge away with increasing resolution. Strategies to obtain initial data of interest are discussed in the subsection 2.2 next. To be sure that initial data give rise to a time development that can be reliably calculated by numerical methods, we must understand whether or not the evolution PDE we are solving is well-posed. Well-posedness is the requirement that a PDE problem admits a unique solution that depends continuously on the given data. This is discussed for evolution problems in

subsection 2.3. The choice of gauge has a direct effect on well-posedness, and so is fundamental in the construction of the free-evolution formulations of GR. This freedom is discussed below in subsection 2.4.

2.2 Initial Data

Our aim in the construction of initial data is to find a configuration of the variables that models a physical scenario of interest whilst simultaneously solving the Hamiltonian and momentum constraints. To fulfill the former condition it is often advantageous to append additional equations to the constraints to impose physical restrictions on the data. To keep the discussion here brief, we review only the most common approach.

As we saw above, the Hamiltonian and momentum constraints

$$\begin{aligned} R + K^2 - K^{ab}K_{ab} &= 16\pi\rho, \\ D^b K_{ab} - D_a K &= 8\pi j_a, \end{aligned} \tag{52}$$

restrict the permissible data at each instant of time Σ_t . They are a collection of four equations for the twelve components of the spatial metric, extrinsic curvature and four components of the stress-energy tensor. Since this system of equations is highly under-determined and does not have a fixed PDE character, many different approaches may be taken to find solutions. What all strategies have in common is that decisions must be made about what part of the initial data will be specified, what ‘dependent variables’ will be introduced and solved for, what data will be given to those variables, and where it should be given.

In asymptotically flat spacetimes, the class most prevalent in NR, the metric and extrinsic curvature reduce to the flat-metric far away from a gravitating source. An attractive approach is thus to specify data for the dependent variables at spatial infinity, where they ought to be simple. In practice this means that we would like to solve a boundary value problem. The canonical PDE with a well-posed boundary value problem is the Laplace equation, which is of elliptic type. For these reasons it is popular to formulate the constraints as a system of second order elliptic PDEs and solve a boundary value problem. There are various different approaches even to this, but we shall focus on the archetype, the conformal transverse-traceless decomposition.

We begin by making a conformal decomposition of the metric,

$$\gamma_{ij} = \psi^4 \tilde{\gamma}_{ij}. \tag{53}$$

We use the common convention to raise and lower the indices of objects with a tilde using the inverse conformal metric $\gamma^{ij} = \psi^{-4} \tilde{\gamma}^{ij}$. We denote by \tilde{D}_i the Levi-Civita connection of $\tilde{\gamma}_{ij}$, write the associated curvature as \tilde{R}_{ijkl} , and denote contractions similarly. Straightforward calculations relate the spatial and conformal curvature

scalars

$$R = \psi^{-4} \tilde{R} - 8\psi^{-5} \tilde{\Delta} \psi, \quad (54)$$

where the conformal Laplace operator is $\tilde{\Delta} \equiv \tilde{D}^i \tilde{D}_i$. Plugging this into the Hamiltonian constraint, we obtain an elliptic equation for the dependent variable ψ . Besides the fact that the conformal decomposition naturally introduces an elliptic operator on the conformal factor, it is aesthetically pleasing that in this construction no single metric component is singled out for special treatment.

The momentum constraint contains only one derivative of the extrinsic curvature, and so to render it a second order equation the obvious maneuver is to introduce a potential. This is the transverse-traceless part of the setup. We write the extrinsic curvature as

$$K^{ij} = \psi^{-10} \tilde{A}^{ij} + \frac{1}{3} \gamma^{ij} K, \quad (55)$$

and place the ansatz

$$\tilde{A}^{ij} = \tilde{D}^i \tilde{v}^j + \tilde{D}^j \tilde{v}^i - \frac{2}{3} \tilde{\gamma}^{ij} \tilde{D}_k \tilde{v}^k + \tilde{M}^{ij}, \quad (56)$$

on the conformal trace-free part \tilde{A}_{ij} , with \tilde{M}^{ij} an arbitrary symmetric trace-free tensor. Plugging this into the momentum constraint, we again obtain a second order elliptic equation, this time for the vector potential \tilde{v}^i , albeit with a more complicated elliptic operator

$$\tilde{\Delta}_v \tilde{v}^i = \tilde{\Delta} \tilde{v}^i + \frac{1}{3} \tilde{D}^i (\tilde{D}_j \tilde{v}^j) + \tilde{R}^i_j v^j, \quad (57)$$

than for the conformal factor.

Putting all of this together, the conformal transverse-traceless decomposition gives the constraints the form

$$\begin{aligned} 8\tilde{\Delta} \psi - \tilde{R} \psi + \psi^{-7} \tilde{A}_{ij} \tilde{A}^{ij} - \frac{2}{3} \psi^5 K^2 + 16\pi \psi^5 \rho &= 0, \\ \tilde{\Delta}_v \tilde{v}^i + \tilde{D}_j \tilde{M}^{ij} - \frac{2}{3} \psi^6 \tilde{D}^i K - 8\pi \psi^{10} j^i &= 0. \end{aligned} \quad (58)$$

We choose data for the conformal metric $\tilde{\gamma}_{ij}$, the trace of the extrinsic curvature K , the symmetric trace-free tensor \tilde{M}^{ij} and pick a matter distribution, which will generate ρ and j^i . As mentioned above, in the routine asymptotically flat setting we impose boundary conditions $\psi = 1$ and $v^i = 0$ at spatial infinity and then solve for (ψ, v^i) everywhere on Σ_t . Yet another beautiful property of elliptic equations is that existence theorems, when they can be applied, guarantee that the solution exists on the entire domain.

Once we have a concrete formulation of the constraints we can turn our attention to making a choice of data that represents the scenario we are interested in studying. In doing so there is frequently a trade-off between the mathematical simplicity and accurately capturing this scenario. For instance, working in vacuum $\rho = j_i = 0$, taking the conformal metric flat $\tilde{\gamma}_{ij} = \delta_{ij}$ and choosing $K_{ij} = 0$, the Hamiltonian

constraint reduces to the flat-space Laplace equation and the momentum constraint is trivially fulfilled. The Hamiltonian constraint is then easily solved. This choice of initial data, called Brill-Lindquist data, represents a number of superposed black holes instantaneously at rest. These are evidently modeled after the Schwarzschild solution in isotropic coordinates, which we recall has spatial metric

$$\gamma_{ij}dx^i dx^j = \psi^4(dx^2 + dy^2 + dz^2) = \left(1 + \frac{M}{2r}\right)^4(dx^2 + dy^2 + dz^2), \quad (59)$$

with $r^2 = x^2 + y^2 + z^2$ as usual. Since we are most often interested in black holes in orbit around each other, this is too restrictive. Working in vacuum with the same conformally flat metric, choosing $K = 0$, called maximal slicing, and $\vec{M}^{ij} = 0$, the momentum constraint decouples from the conformal factor and admits an exact solution, called the Bowen-York solution. This can be used to give linear momentum and spin to the black holes, with the price that the Hamiltonian constraint remains a nonlinear PDE. To solve it we turn then to numerical methods. These data are called ‘puncture-initial data’. They are among the most used binary black hole configurations. Thus, Schwarzschild written in isotropic coordinates serves as the prototype for one of the two main classes of black hole initial data. Again the assumptions placed to simplify the constraints are a direct shortcoming, since neither instants of time in the Schwarzschild spacetime that carry linear momentum nor time slices of the Kerr spacetime can be conformally flat. The prototype for the second class of black hole initial data, called excision data, is the Schwarzschild solution written in horizon penetrating coordinates. The basic idea for the time-evolution of this data is that, since the interior of the black hole can not effect what happens outside, we may cut the black hole region out of the computational domain. See below for a short discussion of what this entails. For excision initial data it is more common to drop the assumptions of conformal flatness and maximal slicing. Likewise when using more sophisticated physical input such as that from Post-Newtonian theory [8], simplifying mathematical assumptions must be abandoned. In that case, the system (58) remains coupled and so requires a general purpose numerical solver for elliptic systems. For an up-to-date review of what is known rigorously for this complete system, see [9].

Setting up initial data for systems including fluid matter poses its own complications. Initial data that are co-rotational or irrotational can be constructed using the clean procedure as presented in [4]. But for generic binary configurations it is common to boost numerically constructed Tolman–Oppenheimer–Volkoff (TOV) configurations to help construct the given data for whatever formulation of the constraints (most often the extended-conformal-thin-sandwich system) is being used. Another subtlety lies at the treatment of the stellar surface, where the Euler equations become formally singular. Further discussion of this can be found in the review article [10].

2.3 Well-posedness of time evolution PDEs

The complete specification of a PDE problem consists of the domain on which the problem is to be solved, the data that is given and of course the PDEs themselves. If a PDE problem admits a unique solution that depends continuously on the given data in some norm we say that the problem is well-posed (with respect to that norm). Well-posedness is a fundamental requirement on a PDE problem, and is of practical concern for numerical approximation. If a PDE is ill-posed, that is, if there exists no norm in which it is well-posed, then solutions of any approximation scheme will fail to converge to the continuum solution (if it even exists) in the limit of infinite resolution.

In this subsection we state without proof the most relevant well-posedness results for the initial value problem and initial boundary value problem. For proofs, together with a numerical perspective, we recommend the classic textbooks [11, 12]. For a discussion closest to the language and needs of NR, we suggest [13, 14], the fascinating review [15], and for a pure mathematical treatment [16]. For an introduction to the long-term behavior of nonlinear wave equations, we also recommend [17].

Consider the first order linear constant coefficient evolution system

$$\partial_t \mathbf{u} = \mathbf{A}^p \partial_p \mathbf{u} + \mathbf{s}. \quad (60)$$

The principal part of the system consists just of the terms involving the highest derivatives. We assume that the components of the state vector \mathbf{u} , the principal part matrices \mathbf{A}^p and the source terms \mathbf{s} are real. Observe that the source terms could be of the form $\mathbf{s} = \mathbf{B}\mathbf{u} + \mathbf{s}'$. The initial value problem consists of setting data,

$$\mathbf{u}(0, x) = \mathbf{f}(x), \quad (61)$$

and requesting a solution at times $t > 0$. In this context, well-posedness of the initial value problem in a norm $\|\cdot\|$ can be characterized by the existence of positive constants α, K such that an estimate

$$\|\mathbf{u}(t, \cdot)\| \leq K e^{\alpha t} \|\mathbf{f}(\cdot)\| \quad (62)$$

holds regardless of the choice of initial data.

Let s_p denote an arbitrary unit spatial covector. The principal symbol \mathbf{P}^s in the s_p direction is defined by $\mathbf{P}^s = \mathbf{A}^s \equiv \mathbf{A}^p s_p$. The system (60) is called weakly hyperbolic if, for every such covector, the principal symbol has real eigenvalues. These can be interpreted as the speeds of propagation of the system. If, furthermore, for every s_p the principal symbol has a complete set of eigenvectors and the bound

$$|\mathbf{T}_s| + |\mathbf{T}_s^{-1}| \leq K, \quad (63)$$

holds uniformly in the direction s_p for some $K > 0$, then we say that the system is strongly hyperbolic. Here \mathbf{T}_s is the matrix that takes the right eigenvectors as columns and where $|\cdot|$ denotes here the spectral norm of a matrix. If there exists a

symmetrizer \mathbf{H} for the system, a symmetric positive definite matrix such that $\mathbf{H}\mathbf{A}^p$ is symmetric for each p , we say that the system is symmetric hyperbolic. Symmetric hyperbolicity is yet a stronger condition than strong hyperbolicity.

The first, crucial theorem is that the initial value problem for the system (60) is well-posed in L^2

$$\|\mathbf{u}(t, \cdot)\|_{L^2}^2 = \int_{\Sigma_t} dx \mathbf{u}(t, x)^T \mathbf{u}(t, x) \quad (64)$$

if and only if it is strongly hyperbolic. We denote the transpose by superscript T . Interestingly, if the system is only weakly hyperbolic, it may be well-posed in a norm that contains specific derivatives of the certain components of the state vector. In contrast to L^2 well-posedness for strongly hyperbolic systems however, the weakly hyperbolic system is sensitive to changes in the source terms \mathbf{s} , and well-posedness is therefore delicate to verify in practice. The second important result is that, for the initial boundary value problem, which consists of specifying initial data on a partial Cauchy slice at $t = 0$ together with boundary conditions at the boundary of the domain at each time, there is a simple prescription to choose boundary conditions such that the problem becomes well-posed when the system (60) is symmetric hyperbolic. This straightforward approach is made possible by the fact that symmetric hyperbolic systems admit energy estimates like (62) by simple physical space arguments involving the divergence theorem, without having to use the Fourier-transform. We demonstrate this below for the wave equation. In GR the application of this result for the initial boundary value problem is greatly complicated by the constraints. The reason for this is that, just as we need to choose initial data that satisfies the constraints, so do we have to choose boundary conditions that are constraint preserving. Likewise, boundary conditions need to be chosen so that they model the physics we are interested in studying. For instance, reflecting boundary conditions are less favored than those which can absorb outgoing waves.

There are obvious differences between the simple system considered in this section and the field equations of GR. First, the formulations of GR we have seen are not first order in all derivatives but rather, first order in time and second order in space. This is purely a technical detail, however, which can be overcome introducing a first order reduction and then applying the definitions as given here. An elementary example of this is given already by the wave equation, discussed momentarily, for which it is easy to see that there is a symmetric hyperbolic first order reduction. Second, the Einstein equations are not linear. This can be surmounted by linearizing about an arbitrary background and then working in a small neighborhood of a point, where to a good approximation the coefficients in the linearized problem will be constant, and we can apply the definitions given in this section. This is known as the localization principle. With additional smoothness assumptions, strong hyperbolicity still guarantees *local well-posedness* in a certain norm. The price we pay for linearization and working just in the neighborhood of each point is that, without investing much more work, we can only guarantee existence of the solution for a short time. Naturally, long-term behavior of solutions is a relevant question of great interest, and one on which much progress is being made. But from a pure NR per-

spective, it is the property of local well-posedness that determines whether or not we can hope to accurately approximate solutions computationally. There is much to say about all this, but to avoid a lengthy discussion, we direct the interested reader to the references highlighted above.

The canonical example of a PDE with a well-posed Cauchy problem is the wave equation in flat-space, which we now consider as a simple example. The wave equation is given by

$$\square_{\eta} \phi = \eta^{ab} \nabla_a \nabla_b \phi = -\partial_t^2 \phi + \partial^i \partial_i \phi = 0, \quad (65)$$

where here \square_{η} is the d'Alembert operator associated with the Minkowski metric, ∇_a is the Levi-Civita derivative of η_{ab} and in the second equality we assume that the coordinates are global inertial. We can draw a crude analogy between GR and the wave equation in which this is identified with the fully second order form of the field equations (1). Introducing the time reduction variable $\pi = -\partial_t \phi$, we can write the system in first-order-in-time-second-order-in-space form

$$\partial_t \phi = -\pi, \quad \partial_t \pi = -\partial^i \partial_i \phi. \quad (66)$$

In analogy to our treatment of GR, this is like the evolution equations (48). We can then reduce the system to first order by introducing the spatial reduction variable Φ_i and the reduction constraint

$$C_i = \partial_i \phi - \Phi_i = 0. \quad (67)$$

Even in the linear constant coefficient setting, not every PDE will admit a first order reduction of the type (60). Such PDEs are not hyperbolic. The canonical example of this is the heat equation $\partial_t \phi = \partial^i \partial_i \phi$. In first order form, the wave equation can be rewritten as

$$\partial_t \phi = -\pi, \quad \partial_t \Phi_i = -\partial_i \pi, \quad \partial_t \pi = -\partial^i \Phi_i. \quad (68)$$

Solutions of the reduction agree with those of the wave equation whenever the reduction constraint (67) is satisfied. We did not introduce a first order reduction of GR, but can perfectly easily do so. In common with what we saw above for GR however, if the reduction constraint is initially satisfied, it will remain so, since we can easily show that $\partial_t C_i = 0$. Taking the state vector to be $\mathbf{u} = (\phi, \Phi_i, \pi)^T$, in the notation of (60), we have

$$\mathbf{A}^p = \begin{pmatrix} 0 & 0 & 0 \\ 0 & 0 & -\delta_i^p \\ 0 & -\delta^{jp} & 0 \end{pmatrix}, \quad \mathbf{s} = \begin{pmatrix} -\pi \\ 0 \\ 0 \end{pmatrix}. \quad (69)$$

The principal symbol \mathbf{P}^s is then

$$\mathbf{P}^s = \mathbf{A}^p s_p = \begin{pmatrix} 0 & 0 & 0 \\ 0 & 0 & -s_i \\ 0 & -s^j & 0 \end{pmatrix}. \quad (70)$$

It has real eigenvalues $0, \pm 1$, and so the reduction is at least weakly hyperbolic. The eigenvectors of \mathbf{P}^s are complete. They are given by

$$\mathbf{u}_0 = (1, 0_j, 0)^T, \quad \mathbf{u}_A = (0, v_j^A, 0), \quad \mathbf{u}_\pm = (0, s_j, \pm 1), \quad (71)$$

where we have introduced two orthogonal unit covectors v_j^A for $A = 1, 2$ that are orthogonal to s_i . The uniformity condition (63) is satisfied with $K = 1$. In this case the principal matrices are already symmetric, so we can choose the symmetrizer $\mathbf{H} = \mathbf{1}$, the 5×5 identity.

Consider the following norm for our first order reduction of the wave equation

$$E(t, \mathbf{u}) = \int_{\Sigma_t} dx \mathbf{u}(t, x)^T \mathbf{H} \mathbf{u}(t, x). \quad (72)$$

In the present context this corresponds almost exactly to the physical energy of the solution. For this reason estimates that hold for such norms are often referred to as energy estimates. Taking a time derivative of (72), substituting the equations of motion and rearranging, we obtain

$$\partial_t E(t, \mathbf{u}) \leq E(t, \mathbf{u}) + \int dx \partial_p (\mathbf{u}(t, x)^T \mathbf{H} \mathbf{A}^p \mathbf{u}(t, x)). \quad (73)$$

Using the divergence theorem to remove the second term, and a simple application of Grönwall's lemma, we conclude with a well-posedness estimate

$$E(t, \mathbf{u})^{1/2} \leq e^{t/2} E(0, \mathbf{f})^{1/2}, \quad (74)$$

with initial data $\mathbf{u}(0, x) = \mathbf{f}(x)$. This is precisely of the form (62) in the L^2 norm. The computations to obtain estimates for an arbitrary symmetric hyperbolic PDE are identical in spirit.

There are various PDE setups of interest in NR besides the initial and initial boundary value problems. Most important are the characteristic initial and characteristic initial boundary value problems, and the hyperboloidal initial value problem. For an introduction to these, see [18, 19, 20].

In the following section, besides presenting the equations themselves, we give a summary of the status of the initial and initial boundary value problems for the most popular formulations of GR in use in NR.

2.4 Free-Evolution Formulations of GR

We saw in section 2.1 that the constraint subsystem for the ADM evolution equations (48) is closed. If we modify the evolution equations by adding combinations of the constraints, this property still holds. We also saw that the field equations of GR do not by themselves impose a choice for the lapse and shift. Thus there is a large freedom in the choice of equations to be solved. A concrete choice for these is known as a (free-evolution) formulation of GR. We observed in section 2.3 that for sufficiently smooth initial data, strong hyperbolicity guarantees local well-posedness of the Cauchy problem. Taking these considerations together, we are guided when constructing formulations of GR to impose *at least* strong hyperbolicity. Such a formulation is often called a hyperbolic reduction. But there are issues besides this. It is highly desirable to obtain gauge conditions that are flexible enough to reliably treat a large range of scenarios of interest. A clever choice of evolved variables can moreover help to reduce numerical error in applications, or even to make it possible to treat data otherwise out of reach.

The basic ingredients in the construction of free-evolution formulations are first, to make a choice of gauge, second, the definition of auxiliary constraints, and finally the choice of coupling between the field equations and the complete set of constraints. These are already well-illustrated by the archetypal example of a hyperbolic formulation of GR, the generalized harmonic gauge formulation. To construct this, let us begin with the trace-reversed Einstein equations written out, in coordinates x^μ defined as in section 2.1, in the form,

$$\begin{aligned} R_{\alpha\beta} &= -\frac{1}{2}g^{\mu\nu}\partial_\mu\partial_\nu g_{\alpha\beta} + \partial_{(\alpha}{}^{(4)}\Gamma_{\beta)} - {}^{(4)}\Gamma^\gamma{}_{\alpha\beta}{}^{(4)}\Gamma_\gamma \\ &\quad + g^{\mu\nu}g^{\delta\varepsilon}\left(\partial_\delta g_{\mu\alpha}\partial_\varepsilon g_{\nu\beta} - {}^{(4)}\Gamma_{\alpha\mu\delta}{}^{(4)}\Gamma_{\beta\nu\varepsilon}\right) \\ &= 8\pi\left(T_{\alpha\beta} - \frac{1}{2}g_{\alpha\beta}T\right), \end{aligned} \tag{75}$$

where we introduce the contracted Christoffel symbols ${}^{(4)}\Gamma_\alpha = g^{\mu\nu}{}^{(4)}\Gamma_{\alpha\mu\nu}$. Comparing the principal part with the wave equation (65), we see that there would be a strong structural similarity if only the second term in the right-hand side, the gradient of the contracted Christoffel symbol were absent. Of course we are not free to simply change the equations to be solved. But looking more closely we realize that the contracted Christoffel symbol can be written as,

$${}^{(4)}\Gamma_\alpha = -g_{\alpha\beta}\square_g x^\beta, \tag{76}$$

with $\square_g = \nabla^a\nabla_a$ here the curved space d'Alembertian. Therefore, we might work with generalized harmonic, also called generalized wave, coordinates

$$\square_g x^\alpha = H^\alpha(x, g). \tag{77}$$

When the gauge source functions $H^\alpha(x, g)$ vanish, these are called harmonic coordinates or wave coordinates. Substituting this expression back into (75) directly and

using the fact that the gauge source functions depend upon the metric, but not partial derivatives of the metric components, the principal part of the equations indeed agrees with that of the curved space wave equation. Formally this is achieved by defining the auxiliary Harmonic constraints

$$C_\alpha = {}^{(4)}\Gamma_\alpha + H_\alpha = 0, \quad (78)$$

and replacing the Einstein equations by the reduced field equations

$$\begin{aligned} \mathcal{R}_{\alpha\beta} &= R_{\alpha\beta} - \nabla_{(\alpha} C_{\beta)} \\ &= -\frac{1}{2}g^{\mu\nu}\partial_\mu\partial_\nu g_{\alpha\beta} + \nabla_{(\alpha} H_{\beta)} \\ &\quad + g^{\mu\nu}g^{\delta\epsilon}\left(\partial_\delta g_{\mu\alpha}\partial_\epsilon g_{\nu\beta} - {}^{(4)}\Gamma_{\alpha\mu\delta}{}^{(4)}\Gamma_{\beta\nu\epsilon}\right) \\ &= 8\pi\left(T_{\alpha\beta} - \frac{1}{2}g_{\alpha\beta}T\right), \end{aligned} \quad (79)$$

where $\mathcal{R}_{\alpha\beta}$ is called the reduced Ricci tensor. This is called the generalized harmonic gauge (GHG) formulation of GR. Due to the similarity with the wave equation discussed in the last section, it is not surprising that the GHG formulation admits a symmetric hyperbolic first order reduction, and thus has a well-posed Cauchy problem. The terminology ‘reduced’ arose as an abbreviation of hyperbolic reduction. To see that the constraint subsystem remains closed, we reverse the trace once more to obtain

$$G_{ab} - \nabla_{(a} C_{b)} + \frac{1}{2}g_{ab}(\nabla_c C^c) = 8\pi T_{ab}. \quad (80)$$

Contracting then with the normal vector n^a and employing the language of the 3+1 decomposition once more, a short calculation gives

$$\begin{aligned} \mathcal{L}_t C_n &= \alpha[H - D_a(\perp C^a) + a^a(\perp C_a) - 2KC_n] + \mathcal{L}_\beta C_n, \\ \perp\mathcal{L}_t(\perp C)_a &= \alpha[2M_a - D_a C_n + a_a C_n - 2K_a{}^b(\perp C)_b] + \perp\mathcal{L}_\beta(\perp C)_a, \end{aligned} \quad (81)$$

for $C_n = C_a n^a$ and $\perp C_a$, so we see that time derivatives of the harmonic constraints are essentially given by the Hamiltonian and momentum constraints we met in section 2.2. Taking the divergence of (80) and using local stress-energy conservation we have

$$\square C_a + R_{ab}C^b = 0, \quad (82)$$

where we can now substitute back from (79) to remove the Ricci tensor. This means that the harmonic constraints satisfy a second order nonlinear wave equation in which every term appears with at least one constraint. Combining this with (81) we can conclude that if we start with constraint satisfying initial data, the time development, which is guaranteed to exist, at least locally, by well-posedness, will satisfy the constraints too.

We have presented GHG formulation itself by returning to the spacetime view, but this was simply because the structure in the equations is more evident in that no-

tation. We can equivalently work with the 3 + 1 language. The harmonic constraints, for instance, can be rewritten as

$$\begin{aligned}\partial_t \alpha &= -\alpha^2(K + C_n + H_n) + \mathcal{L}_\beta \alpha, \\ \partial_t \beta^i &= \alpha^2(\Gamma^i + (\perp C)^i + (\perp H)^i) - \alpha D^i \alpha + \beta^j \partial_j \beta^i.\end{aligned}\quad (83)$$

So it turns out that a choice of gauge as a second order wave equation on the coordinates corresponds to a choice of first order equations of motion for the lapse and shift in the 3 + 1 setting, consistent with the interpretation we gave earlier that the lapse and shift encode the freedom in choosing coordinates.

To build the reduced Einstein equations (79), we chose a specific combination of derivatives of constraints to add to the Einstein equations. As we have seen, local well-posedness of hyperbolic PDEs only depends upon the principal part. Therefore one may wonder why we chose to add a symmetrized covariant derivative, which contains non-principal constraint additions. The answer in this case is that the choice we made presently results in the simplest form of the equations, which we hope makes the general strategy more transparent. More generally, one might feel that the use of the Levi-Civita derivative is preferred as it is covariant, but if we take seriously the point of view of [1] then the same applies to partial derivatives. Nevertheless, it is perfectly legitimate to ask whether one non-principal constraint addition or another is to be preferred. In numerical applications, error will generically violate the constraints. Although such violations should converge to zero with increasing resolution, any strategy to suppress them at finite resolution is welcome. The behavior of numerical error reflects to some extent the behavior of the continuum equations. Motivated by this type of reasoning, a crucial adjustment to the formulation (79) for numerical applications was obtained. The idea is to carefully make non-principal constraint additions,

$$\mathcal{R}_{\alpha\beta} = R_{\alpha\beta} - \nabla_{(\alpha} C_{\beta)} + \gamma_0 (n_{(a} C_{b)} - \frac{1}{2} g_{ab} C_c n^c) = 8\pi (T_{\alpha\beta} - \frac{1}{2} g_{\alpha\beta} T). \quad (84)$$

Linearizing, it can be seen that choosing γ_0 positive leads to the exponential suppression of small, high-frequency constraint violations. Combined with the wave-like propagation of the harmonic constraints, this idea is essentially the same as that of hyperbolic divergence cleaning in GRMHD. The use of such constraint damping schemes is now standard with various formulations of GR. Besides this constraint damping scheme, there are various different choices of non-principal constraint addition in use in the NR literature, giving rise to slightly different flavors of the GHG formulation.

The GHG formulation as presented here is often subjected to a first order in time (or even fully first order) reduction when implemented in practice. Together these different flavors of GHG constitute one of the two main types of formulations of GR in regular use for astrophysical work in NR. The GHG formulation is symmetric hyperbolic. As discussed above, this allows for much more straightforward PDE analysis. In particular, this has led to a proof of well-posedness of the initial boundary value problem with boundary conditions that are constraint preserving and

gravitational radiation controlling. The GHG formulation is the only formulation of GR with this property in frequent use in NR simulations that actually uses these boundary conditions in applications.

We now come to the second class of formulations of GR in frequent use for astrophysical NR. In the literature these are referred to as the Baumgarte-Shapiro-Shibata-Nakamura-Oohara-Kojima (BSSNOK or BSSN), CCZ4 and Z4c formulations. All three are constructed following the general template laid out above. They are furthermore closely related and indeed, the latter two are essentially variations of each other, as they share principal part and constraint damping terms. In particular, all three formulations share in common the use of a conformal decomposition in the choice of variables. We will try to give a unified presentation that covers all three simultaneously. We begin with the trace-reversed Einstein equations and, as above, define auxiliary constraints, this time called Z_a . We then replace the Einstein equations by the Z4 equations of motion

$$R_{ab} + 2\nabla_{(a}Z_{b)} - \kappa_1 [2n_{(a}Z_{b)} - (1 + \kappa_2)g_{ab}n_c Z^c] + W_{ab}(Z) = 8\pi(T_{ab} - \frac{1}{2}g_{ab}T), \quad (85)$$

where $W_{ab}(Z)$ is a symmetric tensor that vanishes when $Z_a = 0$, but which is otherwise arbitrary. This tensor parametrizes the different flavors of the formulation. As in the GHG formulation, we have introduced constraint damping terms with parameters κ_1 and κ_2 . Solutions of these equations agree with those of GR when $Z_a = 0$.

Comparing the Z4 equations of motion with (84), there is an obvious similarity. In fact, choosing

$$Z_a = -\frac{1}{2}C_a, \quad \kappa_1 = \gamma_0, \quad \kappa_2 = 0, \quad (86)$$

and taking $W_{ab} = 0$, the expressions align perfectly. The important difference, however, is that in the Z4 setup we have not yet chosen an equation of motion for the lapse and shift. Morally, therefore, we may think of Z4 as a formulation with the same constraint subsystem as GHG, but without imposing generalized harmonic coordinates.

We will follow the common presentation of these conformal variable formulations in using the 3 + 1 language and working in adapted coordinates, writing the components of the equations of motion. We begin by decomposing the Z4 constraint, introducing $\Theta = -n_a Z^a$, and the spatial part Z_i . Geometrically this is defined by application of the projection operator, but in adapted coordinates we can use the components downstairs. The definition of the extrinsic curvature remains unchanged, so we have

$$\partial_t \gamma_{ij} = -2\alpha K_{ij} + \mathcal{L}_\beta \gamma_{ij}, \quad (87)$$

as in the ADM setup above. For the extrinsic curvature itself we simply take the spatial part of (85). This of course gives equations that look like the ADM evolution equations for K_{ij} , plus constraint additions,

$$\begin{aligned} \partial_t K_{ij} = & -D_i D_j \alpha + \alpha \left[R_{ij} - 2K^k{}_i K_{jk} + K K_{ij} + 2D_{(a} Z_{b)} - 2K_{ij} \Theta + W_{ij} \right] \\ & - \alpha \kappa_1 (1 + \kappa_2) \gamma_{ij} \Theta + 4\pi \alpha [\gamma_{ij}(s - \rho) - 2s_{ij}] + \mathcal{L}_\beta K_{ij}. \end{aligned} \quad (88)$$

For the constraints, we trace-reverse (85) and contract with n^a twice (for the Θ equation of motion) and likewise contract once with n^a and once with the projection operator (for the Z_i equation). This gives,

$$\begin{aligned} \partial_t \Theta = & \alpha \left[\frac{1}{2} H + D^i Z_i - a^i Z_i - K \Theta - \kappa_1 (2 + \kappa_2) \Theta + \hat{W}_{nn} \right] + \mathcal{L}_\beta \Theta, \\ \partial_t Z_i = & \alpha \left[M_i + D_i \Theta - a_i \Theta - 2K_i{}^j Z_j - \kappa_1 Z_i - W_{ni} \right] + \mathcal{L}_\beta Z_i. \end{aligned} \quad (89)$$

Where we denote $\hat{W}_{nn} = W_{nn} - W/2$. The complete collection of the constraints is then given by

$$\Theta = 0, \quad Z_i = 0, \quad H = 0, \quad M_i = 0, \quad (90)$$

with the Hamiltonian and momentum constraints defined exactly as earlier in (45) and (46).

To derive the formal evolution equations for the Hamiltonian and momentum constraints, we trace-reverse (85) and take the divergence with ∇_a , then 3 + 1 decompose. Although straightforward, this is considerably lengthier than for the ADM equations. This reveals

$$\begin{aligned} \partial_t H = & -2\alpha D^i M_i - 4M_i D^i \alpha + 2\alpha K H + 4\alpha (K \gamma^{ij} - K^{ij})(D_i Z_j - K_{ij} \Theta + \frac{1}{2} W_{ij}) \\ & - 4\alpha \kappa_1 (1 + \kappa_2) K \Theta + \mathcal{L}_\beta H, \\ \partial_t M_i = & -\frac{1}{2} \alpha D_i H + \alpha K M_i - (D_i \alpha) H + D^j (\alpha (2D_{(i} Z_{j)} - 2K_{ij} \Theta + W_{ij})) \\ & - D_i (\alpha (2D_j Z^j - 2K \Theta + \gamma^{jk} W_{jk})) + 2D_i (\alpha \kappa_1 (1 + \kappa_2) \Theta) + \mathcal{L}_\beta M_i. \end{aligned} \quad (91)$$

As discussed above, the actual evolved variables involve a conformal decomposition not dissimilar to, and historically inspired by, that employed in the treatment of the constraints as outlined in section 2.2. The variables themselves are defined through

$$\begin{aligned} \chi = \gamma^{-1/3}, \quad \tilde{\gamma}_{ij} = \gamma^{-1/3} \gamma_{ij}, \quad \hat{K} = \gamma^{ij} K_{ij} - 2\Theta, \\ \tilde{A}_{ij} = \gamma^{-1/3} (K_{ij} - \frac{1}{3} \gamma_{ij} K), \quad \tilde{\Gamma}^i = 2\tilde{\gamma}^{jj} Z_j + \tilde{\Gamma}_d^i, \quad \tilde{\Gamma}_d^i = \tilde{\gamma}^{jk} \tilde{\Gamma}^i{}_{jk} = \tilde{\gamma}^{jj} \tilde{\gamma}^{kl} \partial_k \tilde{\gamma}_{lj}. \end{aligned} \quad (92)$$

There are minor changes in the choice of variables from one formulation to another, and indeed across different implementations. The key benefit of this change of variables is that they help in the treatment of data in which the metric components blow-up in an isotropic manner. Consider for instance the prototype for puncture-type initial data, the Schwarzschild metric with the usual time coordinate and isotropic coordinates. In that case, all non-vanishing component of the spatial metric (59) diverge as $r \rightarrow 0$, but the evolved metric remains trivial. One would therefore expect that perturbations would give a conformal metric that could also be inverted without

problem. This turns out to be the case in a large variety of situations of interest. Nevertheless, since the determinant of the metric diverges we must still manage one singular variable. In practice this is managed by evolving χ , a negative power of the determinant of the spatial metric, see the definition in (92). The definition of χ thus guarantees that the evolved variable remains finite, although keeping in mind (59) as a model, we may be concerned about the degree of smoothness of solutions when χ vanishes, and moreover any inverse power of χ that appears in the equations of motion. The remaining variables are chosen so that the complete set of equations of motion appear as regular as possible. (There is no proof that this is the optimal choice, but many different choices have been investigated. With carefully chosen numerical methods, even less regular choices of variable may be managed, but the conformal decomposition remains the most prevalent choice to manage this type of data). We see that under this change we have apparently increased the number of evolved variables, but we have also introduced the algebraic constraints

$$\det \tilde{\gamma}_{ij} = \tilde{\gamma} = 1, \quad \tilde{\gamma}^{ij} \tilde{A}_{ij} = \tilde{A} = 0. \quad (93)$$

When these constraints are explicitly enforced, which is typically done in practice, the solution spaces of the evolution equations with either the ADM or the conformal variables are isomorphic and they therefore have shared PDE properties.

Pushing the evolution equations (87), through the change of variables, we obtain

$$\begin{aligned} \partial_t \chi &= \frac{2}{3} \chi [\alpha(\hat{K} + 2\Theta) - D_i \beta^i], \\ \partial_t \tilde{\gamma}_{ij} &= -2\alpha \tilde{A}_{ij} + \beta^k \partial_k \tilde{\gamma}_{ij} + 2\tilde{\gamma}_{k(i} \partial_{j)} \beta^k - \frac{2}{3} \tilde{\gamma}_{ij} \partial_k \beta^k, \end{aligned} \quad (94)$$

Likewise from (89) we have

$$\partial_t \Theta = \alpha \left[\frac{1}{2} H + D^i Z_i - a^i Z_i - K\Theta - \kappa_1(2 + \kappa_2)\Theta + \hat{W}_{nn} \right] + \mathcal{L}_\beta \Theta, \quad (95)$$

for the Θ constraint and the complicated expression

$$\begin{aligned} \partial_t \tilde{\Gamma}^i &= 2\alpha \left[\tilde{\Gamma}^i{}_{jk} \tilde{A}^{jk} - \frac{3}{2} \tilde{A}^{ij} \partial_j \ln \chi - \tilde{A}^{ij} a_j - 4\pi \tilde{\gamma}^{ij} s_j - \frac{1}{3} \tilde{\gamma}^{ij} \partial_j (2\hat{K} + \Theta) \right. \\ &\quad \left. - \frac{1}{3} (\hat{K} + 2\Theta) (\tilde{\Gamma}^i - \tilde{\Gamma}_d^i) - \tilde{\gamma}^{ij} a_j \Theta - \tilde{\gamma}^{ij} W_{jn} \right] - \alpha \kappa_1 (\tilde{\Gamma}^i - \tilde{\Gamma}_d^i) \\ &\quad + \tilde{\gamma}^{jk} \partial_j \partial_k \beta^i + \frac{1}{3} \tilde{\gamma}^{ij} \partial_j \partial_k \beta^k + \beta^j \partial_j \tilde{\Gamma}^i - \tilde{\Gamma}^j \partial_j \beta^i + \frac{2}{3} \tilde{\Gamma}^i \partial_j \beta^j, \end{aligned} \quad (96)$$

when we combine derivatives of (94) with (89). Finally, doing the same for (88), we arrive at

$$\begin{aligned} \partial_t \hat{K} &= -D^i D_i \alpha + \alpha [\tilde{A}^{ij} \tilde{A}_{ij} + \frac{1}{3} (\hat{K} + 2\Theta)^2] + 4\pi \alpha [s + \rho] \\ &\quad + \alpha [2a^i Z_i + K\Theta + 2\kappa_1(1 + \kappa_2)\Theta - W_{nn}] + \mathcal{L}_\beta \hat{K}, \end{aligned} \quad (97)$$

for the trace variable, and

$$\partial_t \tilde{A}_{ij} = \chi \left[-D_i D_j \alpha + \alpha (R_{ij} + 2D_{(i} Z_{j)} + W_{ij} - 8\pi s_{ij}) \right]^{\text{tr}} + \alpha [\hat{K} \tilde{A}_{ij} - 2\tilde{A}^k{}_i \tilde{A}_{jk}]$$

$$+ \beta^k \partial_k \tilde{A}_{ij} + 2\tilde{A}_{k(i} \partial_{j)} \beta^k - \frac{2}{3} \tilde{A}_{ij} \partial_k \beta^k, \quad (98)$$

for the trace-free part of the extrinsic curvature. Here we have employed a number of auxiliary definitions and shorthands. The superscript *tf* denotes the trace-free part as usual. The spatial Christoffel symbols can be expressed in terms of the conformal connection via,

$$\Gamma^k{}_{ij} = \tilde{\Gamma}^k{}_{ij} - \delta^k{}_{(i} \partial_{j)} \ln \chi + \frac{1}{2} \tilde{\gamma}_{ij} \tilde{\gamma}^{kl} \tilde{\partial}_l \ln \chi. \quad (99)$$

In terms of the conformal variables, the spatial Ricci tensor can be expressed as

$$\begin{aligned} R_{ij} &= \tilde{R}_{ij}^\chi + \tilde{R}_{ij}, \\ \tilde{R}_{ij}^\chi &= \frac{1}{2\chi} \tilde{D}_i \tilde{D}_j \chi + \frac{1}{2\chi} \tilde{\gamma}_{ij} \tilde{D}^k \tilde{D}_k \chi - \frac{1}{4\chi^2} \tilde{D}_i \chi \tilde{D}_j \chi - \frac{3}{4\chi^2} \tilde{\gamma}_{ij} \tilde{D}^k \chi \tilde{D}_k \chi, \\ \tilde{R}_{ij} &= -\frac{1}{2} \tilde{\gamma}^{kl} \partial_k \partial_l \tilde{\gamma}_{ij} + \tilde{\gamma}_{k(i} \partial_{j)} \tilde{\Gamma}_d{}^k + \tilde{\Gamma}_d{}^k \tilde{\Gamma}_{(ij)k} + \tilde{\gamma}^{lm} \left(2\tilde{\Gamma}^k{}_{l(i} \tilde{\Gamma}_{j)km} + \tilde{\Gamma}^k{}_{im} \tilde{\Gamma}_{klj} \right), \end{aligned} \quad (100)$$

To summarize, in terms of the conformal variables the Z4 constraints are

$$\Theta = 0, \quad 2Z_i = \tilde{\gamma}_{ij} (\tilde{\Gamma}^j - \tilde{\Gamma}_d{}^j). \quad (101)$$

The Hamiltonian and momentum constraints are

$$\begin{aligned} H &= R - \tilde{A}^{ij} \tilde{A}_{ij} + \frac{2}{3} (\hat{K} + 2\Theta)^2 - 16\pi\rho = 0, \\ \tilde{M}^i &= \tilde{\gamma}^{ij} M_j = \tilde{D}_j \tilde{A}^{ij} - \frac{2}{3} \tilde{D}^i (\hat{K} + 2\Theta) - \frac{3}{2} \tilde{A}^{ij} \tilde{D}_j \ln \chi - 4\pi \tilde{\gamma}^{ij} s_j = 0, \end{aligned} \quad (102)$$

in addition to which we have the algebraic constraints (93), which are assumed to be imposed for the reasons discussed above.

The most popular gauge condition in use with these conformal formulations can be written

$$\begin{aligned} \partial_t \alpha &= -2\alpha \hat{K} + \mathcal{L}_\beta \alpha, \\ \partial_t \beta^i &= \mu_s \tilde{\Gamma}^i - \eta \beta^i + \beta^j \partial_j \beta^i. \end{aligned} \quad (103)$$

This is known as the moving-puncture gauge. Again, there are various different flavors in use, and here we have selected just the simplest. Observe that just as in the GHG formulation, we choose here evolution equations for the lapse and shift, and in fact these look structurally similar to the generalized harmonic choice. The lapse condition is referred to as the ‘1 + log’ variant of the Bona-Massó slicing condition. The shift condition is known as ‘Gamma-driver shift’. In GHG, all of the speeds of propagation associated with the gauge choice coincide with the speed of light. That is not the case in moving puncture gauge, which instead has various superluminal speeds.

Moving now to the constraint addition tensor W_{ab} , observe that we have

$$W_{ab} = n_a n_b W_{nn} - 2n_{(a} \perp W_{b)n} + \frac{1}{3} \gamma_{ab} [2\hat{W}_{nn} - W_{nn}] + \perp W_{ab}^{\text{tf}}. \quad (104)$$

The first of the three common flavors of this ‘conformal decomposition’ setup, which we give in reverse historical order of their appearance, is called CCZ4. In CCZ4 the only non-trivial piece of the constraint addition tensor W_{ab} is taken to be

$$W_{in} = \alpha^{-1}(\kappa_3 - 1) \left(\frac{2}{3} Z_i \partial_k \beta^k - \gamma_{ij} \gamma^{kl} Z_k \partial_l \beta^j \right), \quad (105)$$

often with $\kappa_3 = 1$, but occasionally with $\kappa_3 = 1/2$. One needs to check the literature for details in different cases. CCZ4 is often used with $\chi^{1/2}$ in place of χ as an evolved variable. The second variation is called Z4c, in which the constraint addition tensor is

$$\begin{aligned} W_{nn} &= 2a^i Z_i + K\Theta + \kappa_1(1 + \kappa_2)\Theta, \\ \hat{W}_{nn} &= a^i Z_i + K\Theta + \Gamma^i Z_i - \frac{2}{3} \Gamma^i_{ij} Z^j, \\ \tilde{\gamma}^{ij} W_{jn} &= \frac{1}{3} (\hat{K} + 2\Theta)(\tilde{\Gamma}^i - \tilde{\Gamma}_d^i) + \tilde{\gamma}^{ij} a_j - \alpha^{-1} \tilde{\gamma}^{jk} Z_k \partial_j \beta^i + \frac{2}{3} \alpha^{-1} \tilde{\gamma}^{ij} Z_j \partial_k \beta^k, \\ W_{ij}^{\text{tf}} &= 2\Theta K_{ij}^{\text{tf}} + 2 \left[\Gamma^k_{ij} Z_k - \frac{2}{3} \Gamma^k_{k(i} Z_{j)} \right]^{\text{tf}}. \end{aligned} \quad (106)$$

The reason for these choices was to make the equations of motion as close as possible to those of the following formulation. To obtain the the third popular option, the BSSN formulation (called on occasion BSSNOK), one need only take the Z4c equations of motion, and set

$$\Theta = 0, \quad (107)$$

discarding it as an evolved variable, and set all of the constraint damping parameters κ_1, κ_2 to zero. Further variations, including first order reductions and slightly different choices of variable have been investigated. Observe that here we have sacrificed fidelity to the notation used in the literature to present all three formulations together simultaneously.

With suitable choices for the gauge parameter μ_S in (103) all three variants are strongly hyperbolic and therefore as discussed in section 2.3 admit a well-posed initial value problem. For the moving puncture gauge none are symmetric hyperbolic, and so well-posedness results for the initial boundary value problem are technically harder to come by. Such results are well summarized in [13] (see also [21] for a proof of well-posedness for a system close to those presented here). Consequently most implementations working with puncture gauge employ a naive outer boundary treatment, but try to place the boundary sufficiently far away from the region of interest that it has a negligible effect on the physics of the system.

In the principal part the relationship between gauge, constraints and the gravitational wave degrees of freedom can be understood straightforwardly. It turns out that hyperbolicity of gauge choices can be understood independently of the formulation of GR, and that strong hyperbolicity of a gauge choice is a necessary condition that a formulation built with that gauge will itself be strongly hyperbolic. The same holds for the constraint subsystem.

Supposing we want to tackle a particular physical problem, what principles can we use to choose between different formulations, both here and more generally? In

accordance with our discussion above, a first requirement is that of well-posedness of the initial boundary value problem, ideally with boundary conditions that can be implemented in practice. From this point of view the GHG formulation is preferred over those which use moving puncture gauge. On the other hand, as discussed momentarily, the use of the conformally decomposed variables does give a clear advantage in managing the puncture representation of black holes. As we have seen, there is little difference between the different flavors of conformal decomposition of Z4. Both have a constraint subsystem that looks like the wave equation in the principal part, and accept the same constraint damping scheme as the GHG formulation. Non-principal differences in the constraint subsystem do make a difference to the long-term behavior of constraint violations and can induce exponential growth or worse. The analysis required to understand this for a particular constraint addition is, unfortunately, technically involved, and so there is no systematic understanding of what choices are optimal in general. The wavelike nature and damping scheme for the Z4 constraint subsystem has been shown to give advantages over BSSN computations in certain scenarios. The reason for this is that the BSSN constraint subsystem contains slow speeds, which result in constraint violation that sits stationary on the numerical domain and grows.

A crucial feature of formulations of NR is in how black holes are to be managed. We saw in our discussion of initial data that binary black hole initial data can be modeled on the Schwarzschild solution in isotropic coordinates. These are called puncture initial data. The crucial strength of working with the conformally decomposed variables (92) and the moving-puncture gauge (103) is that the points at which the conformal factor χ vanishes (the puncture) is naturally advected around by the shift condition. In practice this results in a highly versatile treatment with many different physical configurations that requires little fine-tuning of the numerical algorithm. The disadvantage of the moving-puncture approach is the limited regularity of solutions at the puncture itself. Excision, in which the black hole region is cut out of the computational domain explicitly, results in smooth solutions but poses a much greater technical obstacle, since we have to monitor the solution, either actively or passively, to be sure that the excision boundary does not require boundary conditions and that (some notion of) the black hole horizon remains within the computational domain.

3 The Physical Interpretation of Numerical Spacetimes

In most cases the raw solution to the Einstein equations provided by the metric over an extended region of spacetime does not correspond directly to the physical quantity of interest. Instead the data is subjected to post-processing. The key examples of this are black hole horizons and gravitational waves. For brevity, we give only an informal overview of each.

Asymptotically flat spacetimes can be characterized by the existence of a certain region in which the metric can be represented as a perturbation of the Minkowski

metric in global inertial coordinates. In these spacetimes there is a natural notion of future null-infinity, the final destination for outgoing gravitational waves emitted from the strong-field region. The black hole region, if it is non-empty, is defined as the complement of the causal past of future null-infinity. The boundary of the black hole region is called the event horizon. This definition relies on global structure and is therefore not applicable if we are given only a subset of the spacetime without future null-infinity. Provided a large enough region of data, we can nevertheless compute an accurate approximation to the position of the event horizon. In practice this is done by integrating null-geodesics backwards in time to find the points in spacetime around which they accumulate. Since we compute spacetimes in NR forward in time, this procedure has to be done by post-processing data.

To understand the physics during the evolution itself it is often helpful to have a proxy for the event horizon. For this we build on the concept of a trapped surface. A trapped surface within a foliation is a closed surface at a fixed instant of time Σ_t whose area form would decrease from any point on the surface if we dragged that point infinitesimally to the future along an outgoing null-geodesic starting at said point. In case the area form would remain constant under such a deformation, the surface is called marginally trapped. The outermost marginally trapped surface is called the apparent horizon. Trapped surfaces play an important role in the singularity theorems. For the purposes of NR, the most relevant fact is that if we have a spacetime that does not contain naked singularities, as is expected generically in black hole spacetimes, then any trapped surface must lie inside a cross-section of the event horizon. The definition of the apparent horizon refers to instants of time and so appears in different positions in different foliations, but since it is defined locally in time can be used to characterize black holes during a numerical evolution itself. For details of numerical methods for apparent and event horizon searches, see [22]. For details of additional quasilocal quantities that may be used to interpret spacetimes, see [23].

The primary deliverable of NR for gravitational wave astronomy is the gravitational waveform emitted from a compact binary system. The natural mathematical idealization of a distant observer in an asymptotically flat spacetime, which serves as a model observer for experiments, lies at future null-infinity. From the waveform one can compute the total energy and linear momentum emitted from a system. As is the case with the event horizon, since the computational domain does not, in most cases, include future null-infinity, we can not extract this signal from numerical data. Nevertheless, if a sufficiently large domain is chosen an accurate approximation to the signal at infinity can be computed by extrapolation. This wave extraction procedure can be performed in multiple ways but the most popular approach employs the Newman-Penrose formalism. Besides textbook treatments, the review article [24] contains a complete overview. There is an ongoing effort to include future null-infinity in the computational domain [18, 25, 26, 27] in generic asymptotically flat systems. Even with such an improvement, calculating and extracting gravitational waveforms with NR will remain too expensive, and too slow, to make an extremely dense sampling of the solution space. For applications to gravitational wave astronomy, accurate models that aggregate Post-Newtonian, perturbative and NR informa-

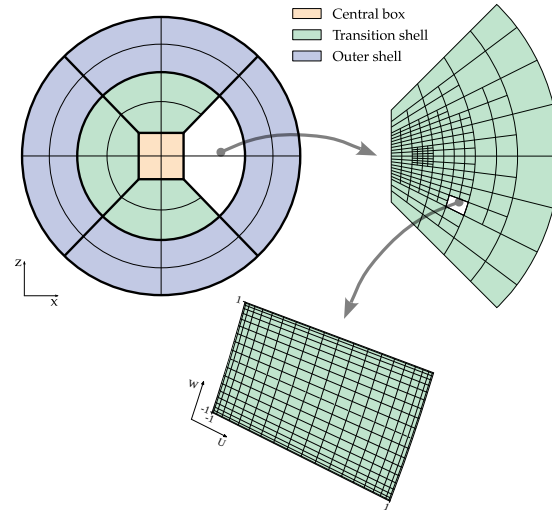


Fig. 2: A simple example of a refined grid structure from a pseudospectral code. Figure taken from [32].

tion are constructed. For textbook introductions to gravitational wave science and modeling, see [28, 29, 30, 31].

4 Numerical Methods, Implementation and Codes

Numerical methods and code engineering for NR is similar to that in other subfields of computational physics, in particular those involving nonlinear PDEs such as computational fluid dynamics and the like.

For time evolution, most common is the use of the method of lines with explicit integrators. This means discretizing in space to obtain a large set of nonlinear ODEs, with one equation per variable for each position on the grid, and the time coordinate as the independent variable. These ODEs are then typically solved with an explicit integration algorithm such as a Runge-Kutta method. The coupling between these different equations is determined by whatever approximation to the spatial derivative is made. For this the most common options are either high-order finite-differencing or pseudospectral methods, in which the grid-function is represented by a basis of orthogonal polynomials. See [33, 34, 35, 36] for textbook introductions to the latter. When working with pseudospectral methods the spatial domain is typically split up into small subdomains, called spectral elements, each of which has an associated initial boundary value problem, with data being communicated from

one element to neighbors using a penalty method. The closely related discontinuous Galerkin method [37] is also becoming more popular in the field.

A qualitative difference between these methods and those used for hydrodynamics is that here a high degree of differentiability is assumed and so there is no mention of shocks or shock capturing. The reason for this is that for systems of nonlinear wave equations, the most natural model for formulations of GR, one expects regularity of solutions to persist unless the solution itself breaks down. Regularity of solutions is of course limited when the field equations are coupled to fluid matter which can form shocks. An introduction to numerical methods to manage such irregular solutions can be found in the textbooks [38, 39, 40, 41]. Numerical simulations employing such methods are discussed later in this volume.

Adaptive-mesh-refinement (AMR) is a staple for applications in 3d NR. The basic idea is to introduce a measure of numerical error and use that to steer the algorithm to place finer grids where they are needed. The most influential method for finite difference codes is the Berger-Oliger method or derivatives thereof. For compact binary systems it is common to use a simplified ‘moving-box’ restriction of this approach. Pseudospectral codes employ instead a hybrid approach in which both the spectral elements are made smaller and the number of basis polynomials is increased. For an illustration of such a refined mesh, see Fig. 2. Although still somewhat niche in NR, impressive progress has been made in using wavelets for AMR [42].

For elliptic boundary value problems such as those we saw emanating from the constraint equations, many of the methods just mentioned for approximating derivatives are employed within iterative schemes that should converge to solutions of the discretized equations at finite resolution. Nonlinearities may be treated by explicit linearization, with preconditioning for the linear solve, under a Newton-Raphson root finding method, and for efficiency multigrid or AMR is again in widespread use.

From an engineering point of view, 3d NR codes are fairly complicated. They are generally designed to be run on supercomputers. Low-level parts of the code are written in a variety of different programming languages including `c`, `c++`, `Fortran` and `Julia`, with code generated using computer algebra packages such as `Mathematica` or `Mathics`. Job sizes vary greatly, but computation on several thousand cores is common. There are numerous paradigms to effectively achieve parallelism, but ultimately to do so the computational domain has to be divided up and split across different processors. To share data between different processing cores the message-passing standard `MPI` is usually used. For shared memory architectures the `openMP` standard is popular. Post-processing, data analysis and the creation of figures is often performed in `Julia`, `Mathematica` or `Python`.

Earlier in the text we asserted that well-posedness of a PDE problem is a necessary condition for an approximation scheme to converge to the continuum solution in the limit of infinite resolution. But what of sufficient conditions? The fact is that in NR there is a considerable gap between what has been proven and that which is implemented and used in practice. The state-of-the-art in this direction is for linear symmetric hyperbolic systems with variable coefficients. There is no proof of

Code	Developers	Resources
AMSS-NCKU	Beijing Normal University	[44]
bam	CoRe Collaboration	[45]
bamps	Jena/Lisbon	[46, 47]
COFFEE	Canterbury/Otago	[48, 49]
Dendro-GR	Brigham-Young/Utah	[50, 42, 51]
Einstein Toolkit	The ET Consortium	[52, 53, 54]
Antelope (FIL)	Frankfurt/Princeton	[55, 56]
Canuda	Aveiro/Illinois	[57, 58, 59]
LazEv	Rochester	[60, 61]
LEAN	Cambridge	[62]
MAYA	Austin	[63, 64]
McLachlan	Louisiana-State/Perimeter	[65, 66]
prague	Charles University Prague	[67, 68]
SphericalNR	Bowdoin/Rochester/West Virginia	[69, 70]
Elliptica	Florida-Atlantic	[71]
ExaHyPE	Frankfurt/Trento	[72, 73]
FUKA	Frankfurt/Paris Observatory/Princeton	[56, 74]
GR-Athena++	Jena/Penn-State/Princeton	[75]
GRCHOMBO	GRTL Collaboration	[76, 77, 78]
HAD	Long-Island	[79, 80, 81]
KADATH	Paris Observatory	[82, 83]
LORENE		[84]
NMESH	Florida-Atlantic	[85]
gh3d2m	Perimeter/Princeton	[86, 87]
SACRA	Illinois/Kyoto/Okinawa/Tsukuba/Toho/Tokyo/Wako	[88]
SENR/NRpy+	University of Idaho	[89]
SpEC		[90]
SpECTRE	SxS Collaboration	[91, 92]
SphGR	Bowdoin	[93, 94]
SPHINCS_BSSN	Hamburg-Louisiana-Stockholm	[95, 96]

Table 1: A collection of 3d NR codes in current use, listed together with their developers and with links to technical descriptions, useful introductions and/or their webpages. We restrict here to tools that solve for the metric. The Einstein Toolkit is a broad infrastructure under which we have placed (indented) important individual projects. The ExaHype code likewise provides infrastructure, but to the best of our knowledge there is only one NR module, which we point to here.

convergence for the nonlinear equations for any of the formulations or discretizations discussed above, even without AMR. See [43] for a textbook introduction to numerical analysis, and [13] for a summary of relevant work in NR. For lack of this we have to rely on convergence series. Numerical results are obtained for the exact same physical configuration but at different resolutions. These data are then compared to establish consistency with convergence to the continuum solution, ideally with an expected rate. With this established, the same data can be used to make error-estimates.

In Table 1 we give a brief overview of the 3d NR codes currently in use. We include here only codes that solve for the metric variables, and only those designed

to treat the initial or initial boundary value problems. A similar summary, which includes also tools for treating fluid matter rather than just focusing on the metric can be found in [97]. For an overview of codes written to solve the characteristic initial boundary value problem for astrophysical applications, see [18, 26, 27]. Tools to manage, post-process and plot data produced by each of these tools are described either within the references or at the associated webpages.

Acknowledgements I am grateful to Jorge Expósito Patiño, Tomas Ledvinka, Christian Peterson Bórquez, Krinio Marouda, Hannes Rüter, Alex Vañó-Viñuales and Miguel Zilhão for helpful discussions and/or feedback on the text. This work was supported in part by FCT (Portugal) Project No. UIDB/00099/2020.

References

1. Robert M. Wald. *General relativity*. The University of Chicago Press, Chicago, 1984.
2. Yosuke Mizuno and Luciano Rezzolla. General-Relativistic Magnetohydrodynamic Equations: the bare essential. 4 2024.
3. Miguel Alcubierre. *Introduction to 3+1 Numerical Relativity*. Oxford University Press, Oxford, 2008.
4. Thomas W. Baumgarte and Stuart L. Shapiro. *Numerical Relativity: Solving Einstein's Equations on the Computer*. Cambridge University Press, Cambridge, 2010.
5. Ericourgoulhon. *3+1 Formalism in General Relativity*. Springer, Berlin, 2012.
6. Masaru Shibata. *Numerical Relativity*. World Scientific, Singapore, 2016.
7. Thomas W. Baumgarte and Stuart L. Shapiro. *Numerical Relativity: Starting from Scratch*. Cambridge University Press, 2021.
8. Eric Poisson and Clifford M Will. *Gravity: Newtonian, Post-Newtonian, Relativistic*. Cambridge University Press, Cambridge, England, 2014.
9. Alessandro Carlotto. The general relativistic constraint equations. *Living Rev. Relativity*, 24:2, 2021.
10. Wolfgang Tichy. The initial value problem as it relates to numerical relativity. *Rept. Prog. Phys.*, 80(2):026901, 2017.
11. Heinz-Otto Kreiss and Jens Lorenz. *Initial-boundary value problems and the Navier-Stokes equations*. Academic Press, New York, 1989.
12. Bertil Gustafsson, Heinz-Otto Kreiss, and Joseph Oliger. *Time dependent problems and difference methods*. Wiley, New York, 1995.
13. Olivier Sarbach and Manuel Tiglio. Continuum and discrete initial-boundary value problems and einstein's field equations. *Living Reviews in Relativity*, 15(9), 2012.
14. David Hilditch. An Introduction to Well-posedness and Free-evolution. *Int. J. Mod. Phys.*, A28:1340015, 2013.
15. Helmut Friedrich and Alan D. Rendall. The Cauchy problem for the Einstein equations. *Lect. Notes Phys.*, 540:127–224, 2000.
16. Hans Ringström. *The Cauchy Problem in General Relativity*. European Mathematical Society, 2009.
17. C.D. Sogge. *Lectures on nonlinear wave equations*. Number Bd. 2 in Monographs in analysis. International Press, 1995.
18. Jeffrey Winicour. Characteristic evolution and matching. *Living Rev. Relativity*, 8:10, 2005. [Online article].
19. Jörg Frauendiener. Conformal infinity. *Living Rev. Relativity*, 7(1), 2004.
20. Juan-Antonio Valiente-Kroon. *Conformal Methods in General Relativity*. Cambridge University Press, Cambridge, 2016.

21. David Hilditch and Milton Ruiz. The initial boundary value problem for free-evolution formulations of General Relativity. 2016.
22. Jonathan Thornburg. Event and apparent horizon finders for 3 + 1 numerical relativity. *Living Rev. Relativity*, 2006. [Online article].
23. László B. Szabados. Quasi-local energy-momentum and angular momentum in GR: A review article. *Living Rev. Relativity*, 12:4, 2009.
24. Nigel T. Bishop and Luciano Rezzolla. Extraction of gravitational waves in numerical relativity. *Living Reviews in Relativity*, 19(1):2, 2016.
25. The Hyperboloidal Research Network: <https://hyperboloid.al/>.
26. C. Reisswig, N. T. Bishop, D. Pollney, and B. Szilagyí. Unambiguous determination of gravitational waveforms from binary black hole mergers. *Phys. Rev. Lett.*, 103:221101, 2009.
27. Sizheng Ma et al. Fully relativistic three-dimensional Cauchy-characteristic matching. 8 2023.
28. Michele Maggiore. *Gravitational Waves. Vol. 1: Theory and Experiments*. Oxford University Press, Oxford, 2007.
29. Jolien D. E. Creighton and Warren G. Anderson. *Gravitational-wave physics and astronomy: An introduction to theory, experiment and data analysis*. 2011.
30. Michele Maggiore. *Gravitational Waves. Vol. 2: Astrophysics and Cosmology*. Oxford University Press, 3 2018.
31. N. Andersson. *Gravitational-Wave Astronomy: Exploring the Dark Side of the Universe*. Oxford Graduate Texts. Oxford University Press, 2019.
32. Daniela Cors, Sarah Renkhoff, Hannes R. Rüter, David Hilditch, and Bernd Brügmann. Formulation improvements for critical collapse simulations. *Phys. Rev. D*, 108(12):124021, 2023.
33. Lloyd N. Trefethen. *Spectral Methods in MATLAB*. SIAM, Philadelphia, 2000.
34. John P. Boyd. *Chebyshev and Fourier Spectral Methods (Second Edition, Revised)*. Dover Publications, New York, 2001.
35. Jan S. Hesthaven, Sigal Gottlieb, and David Gottlieb. *Spectral Methods for Time-Dependent Problems*. Cambridge University Press, Cambridge, 2007.
36. David A. Kopriva. *Implementing Spectral Methods for Partial Differential Equations*. Springer, New York, 2009.
37. Jan S. Hesthaven and Tim Warburton. *Nodal Discontinuous Galerkin Methods*. Springer, New York, 2008.
38. R. J. LeVeque. *Numerical Methods for Conservation Laws*. Birkhauser Verlag, Basel, 1992.
39. Randall J. LeVeque. *Finite Volume Methods for Hyperbolic Problems*. Cambridge University Press, 2002.
40. James R. Wilson and Grant J. Mathews. *Relativistic numerical hydrodynamics*. Cambridge University Press, 2003.
41. Luciano Rezzolla and Olindo Zanotti. *Relativistic Hydrodynamics*. Oxford University Press, Oxford, 2013.
42. Milinda Fernando, David Neilsen, Yosef Zlochower, Eric W. Hirschmann, and Hari Sundar. Massively parallel simulations of binary black holes with adaptive wavelet multiresolution. *Phys. Rev. D*, 107(6):064035, 2023.
43. J.W. Thomas. *Numerical Partial Differential Equations: Finite Difference Methods*. Texts in Applied Mathematics. Springer New York, 1998.
44. Zhou-jian Cao, Hwei-Jang Yo, and Jui-Ping Yu. A Reinvestigation of Moving Punctured Black Holes with a New Code. *Phys. Rev. D*, 78:124011, 2008.
45. Core collaboration. <http://www.computational-relativity.org/>.
46. David Hilditch, Andreas Weyhausen, and Bernd Brügmann. Pseudospectral method for gravitational wave collapse. *Phys. Rev. D*, 93(6):063006, 2016.
47. Sarah Renkhoff, Daniela Cors, David Hilditch, and Bernd Brügmann. Adaptive hp refinement for spectral elements in numerical relativity. *Phys. Rev. D*, 107:104043, May 2023.
48. Jörg Frauendiener and Chris Stevens. The non-linear perturbation of a black hole by gravitational waves. I. The Bondi–Sachs mass loss. *Class. Quant. Grav.*, 38(19):194002, 2021.
49. Georgios Doulis, Jörg Frauendiener, Chris Stevens, and Ben Whale. COFFEE – An MPI-parallelized Python package for the numerical evolution of differential equations. *SoftwareX*, 10:100283, 2019.

50. Milinda Fernando, David Neilsen, Hyun Lim, Eric Hirschmann, and Hari Sundar. Massively Parallel Simulations of Binary Black Hole Intermediate-Mass-Ratio Inspirals. *SIAM J. Sci. Comput.*, 41(2):C97–C138, 2019.
51. Dendro-gr website. <https://paralab.github.io/Dendro-GR/>.
52. Frank Löffler, Joshua Faber, Eloisa Bentivegna, Tanja Bode, Peter Diener, Roland Haas, Ian Hinder, Bruno C Mundim, Christian D Ott, Erik Schnetter, Gabrielle Allen Allen, Manuela Campanelli, and Pablo Laguna. The Einstein Toolkit: A Community Computational Infrastructure for Relativistic Astrophysics. *Class. Quant. Grav.*, 29:115001, 2012.
53. Miguel Zilhão and Frank Löffler. An Introduction to the Einstein Toolkit. *Int. J. Mod. Phys. A*, 28:1340014, 2013.
54. Einstein Toolkit.
55. Elias R. Most, L. Jens Papenfort, and Luciano Rezzolla. Beyond second-order convergence in simulations of magnetized binary neutron stars with realistic microphysics. *Mon. Not. Roy. Astron. Soc.*, 490(3):3588–3600, 2019.
56. L. Jens Papenfort, Samuel D. Tootle, Philippe Grandclément, Elias R. Most, and Luciano Rezzolla. New public code for initial data of unequal-mass, spinning compact-object binaries. *Phys. Rev. D*, 104(2):024057, 2021.
57. Hirotada Okawa, Helvi Witek, and Vitor Cardoso. Black holes and fundamental fields in Numerical Relativity: initial data construction and evolution of bound states. *Phys. Rev. D*, 89(10):104032, 2014.
58. Miguel Zilhão, Helvi Witek, and Vitor Cardoso. Nonlinear interactions between black holes and Proca fields. *Class. Quant. Grav.*, 32:234003, 2015.
59. Canuda, <https://bitbucket.org/canuda/>.
60. Manuela Campanelli, Carlos O. Lousto, Pedro Marronetti, and Yosef Zlochower. Accurate evolutions of orbiting black-hole binaries without excision. *Phys. Rev. Lett.*, 96:111101, 2006.
61. Y. Zlochower, J. G. Baker, M. Campanelli, and C. O. Lousto. Accurate black hole evolutions by fourth-order numerical relativity. *Phys. Rev. D*, 72:024021, 2005. gr-qc/0505055.
62. Ulrich Sperhake. Binary black-hole evolutions of excision and puncture data. *Phys. Rev.*, D76:104015, 2007.
63. Karan Jani, James Healy, James A. Clark, Lionel London, Pablo Laguna, and Deirdre Shoemaker. Georgia Tech Catalog of Gravitational Waveforms. *Class. Quant. Grav.*, 33(20):204001, 2016.
64. Deborah Ferguson et al. Second MAYA Catalog of Binary Black Hole Numerical Relativity Waveforms. 9 2023.
65. J. David Brown, Peter Diener, Olivier Sarbach, Erik Schnetter, and Manuel Tiglio. Turduckening black holes: An Analytical and computational study. *Phys. Rev. D*, 79:044023, 2009.
66. C. Reisswig, C. D. Ott, U. Sperhake, and E. Schnetter. Gravitational Wave Extraction in Simulations of Rotating Stellar Core Collapse. *Phys. Rev. D*, 83:064008, 2011.
67. Anton Khirnov and Tomáš Ledvinka. Slicing conditions for axisymmetric gravitational collapse of Brill waves. *Class. Quant. Grav.*, 35(21):215003, 2018.
68. Tomáš Ledvinka and Anton Khirnov. Universality of curvature invariants in critical vacuum gravitational collapse. *Phys. Rev. Lett.*, 127:011104, Jul 2021.
69. Vassilios Mewes, Yosef Zlochower, Manuela Campanelli, Ian Ruchlin, Zachariah B. Etienne, and Thomas W. Baumgarte. Numerical relativity in spherical coordinates with the Einstein Toolkit. *Phys. Rev. D*, 97(8):084059, 2018.
70. Vassilios Mewes, Yosef Zlochower, Manuela Campanelli, Thomas W. Baumgarte, Zachariah B. Etienne, Federico G. Lopez Armengol, and Federico Cipolletta. Numerical relativity in spherical coordinates: A new dynamical spacetime and general relativistic MHD evolution framework for the Einstein Toolkit. *Phys. Rev. D*, 101(10):104007, 2020.
71. Alireza Rashti, Francesco Maria Fabbri, Bernd Brügmann, Swami Vivekanandji Chaurasia, Tim Dietrich, Maximiliano Ujevic, and Wolfgang Tichy. New pseudospectral code for the construction of initial data. *Phys. Rev. D*, 105(10):104027, 2022.
72. Michael Dumbser, Federico Guercilena, Sven Köppel, Luciano Rezzolla, and Olindo Zanotti. Conformal and covariant Z4 formulation of the Einstein equations: strongly hyperbolic first-order reduction and solution with discontinuous Galerkin schemes. *Phys. Rev.*, D97(8):084053, 2018.

73. www.exahype.org/.
74. <https://bitbucket.org/fukaws/workspace/repositories/>.
75. Boris Daszuta, Francesco Zappa, William Cook, David Radice, Sebastiano Bernuzzi, and Viktoriya Morozova. GR-Athena++: Puncture evolutions on vertex-centered oct-tree adaptive mesh refinement. *Astrophys. J. Supp.*, 257(2):25, 2021.
76. Katy Clough, Pau Figueras, Hal Finkel, Markus Kunesch, Eugene A. Lim, and Saran Tunyasuvunakool. GRChombo : Numerical Relativity with Adaptive Mesh Refinement. *Class. Quant. Grav.*, 32(24):245011, 2015.
77. Tomas Andrade et al. GRChombo: An adaptable numerical relativity code for fundamental physics. *J. Open Source Softw.*, 6(68):3703, 2021.
78. Grtl collaboration. <https://www.grchombo.org/>.
79. Steven L. Liebling. The singularity threshold of the nonlinear sigma model using 3D adaptive mesh refinement. *Phys. Rev. D*, 66:041703(R), 2002.
80. Luis Lehner, Steven L. Liebling, and Oscar Reula. AMR, stability and higher accuracy. 2005.
81. <http://had.liu.edu/>.
82. Philippe Grandclément. Kadath: A Spectral solver for theoretical physics. *J. Comput. Phys.*, 229:3334–3357, 2010.
83. <https://kadath.obspm.fr/>.
84. Ericourgoulhon, Philippe Grandclément, Jean-Alain Marck, Jérôme Novak, and Keisuke Taniguchi. <http://www.lorene.obspm.fr>.
85. Wolfgang Tichy, Liwei Ji, Ananya Adhikari, Alireza Rashti, and Michal Pirog. The new discontinuous Galerkin methods based numerical relativity program Nmesh. *Class. Quant. Grav.*, 40(2):025004, 2023.
86. Frans Pretorius. Numerical relativity using a generalized harmonic decomposition. *Class. Quant. Grav.*, 22:425–451, 2005.
87. William E. East, Frans Pretorius, and Branson C. Stephens. Hydrodynamics in full general relativity with conservative AMR. *Phys. Rev.*, D85:124010, 2012.
88. Tetsuro Yamamoto, Masaru Shibata, and Keisuke Taniguchi. Simulating coalescing compact binaries by a new code SACRA. *Phys. Rev.*, D78:064054, 2008.
89. Ian Ruchlin, Zachariah B. Etienne, and Thomas W. Baumgarte. SENR/NRPy+: Numerical Relativity in Singular Curvilinear Coordinate Systems. *Phys. Rev.*, D97(6):064036, 2018.
90. SpEC - Spectral Einstein Code, <http://www.black-holes.org/SpEC.html>.
91. Lawrence E. Kidder et al. SpECTRE: A Task-based Discontinuous Galerkin Code for Relativistic Astrophysics. *J. Comput. Phys.*, 335:84–114, 2017.
92. <https://spectre-code.org/>.
93. Thomas W. Baumgarte, Pedro J. Montero, Isabel Cordero-Carrion, and Ewald Muller. Numerical Relativity in Spherical Polar Coordinates: Evolution Calculations with the BSSN Formulation. *Phys. Rev. D*, 87(4):044026, 2013.
94. Thomas W. Baumgarte, Pedro J. Montero, and Ewald Müller. Numerical Relativity in Spherical Polar Coordinates: Off-center Simulations. *Phys. Rev. D*, 91(6):064035, 2015.
95. S. Rosswog and P. Diener. SPHINCS_BSSN: A general relativistic Smooth Particle Hydrodynamics code for dynamical spacetimes. *Class. Quant. Grav.*, 38(11):115002, 2021.
96. Stephan Rosswog, Francesco Torsello, and Peter Diener. The Lagrangian Numerical Relativity code SPHINCS_BSSN_v1.0. 6 2023.
97. Niayesh Afshordi et al. Waveform Modelling for the Laser Interferometer Space Antenna. 11 2023.